



Characteristic lengths in natural bundle assemblies arising from fiber-matrix energy competition: A floquet-based homogenization theory



Fabio Manca ^{a, b}, Pier Luca Palla ^{a, c}, Fabrizio Cleri ^{a, c}, Stefano Giordano ^{a, b, *}

^a Institute of Electronics, Microelectronics and Nanotechnology (IEMN UMR CNRS 8520), 59652 Villeneuve d'Ascq, France

^b Joint International Laboratory LIA LEMAC/LICS, École Centrale de Lille, ComUE Lille Nord de France, 59652 Villeneuve d'Ascq, France

^c University of Lille 1, Science and Technology, 59652 Villeneuve d'Ascq, France

ARTICLE INFO

Article history:

Received 19 January 2016

Received in revised form

29 April 2016

Accepted 13 July 2016

Available online 19 July 2016

Keywords:

Fiber bundle

Periodically heterogeneous material

Homogenization

Optimization

Length scale

ABSTRACT

The physical heterogeneity and the geometrical periodicity of several bundle architectures found in biological materials play a key role in determining their superior mechanical performances. The underlying mechanism is based on the shear stress transfer between hard fibers and soft matrix. This process yields a size-dependent behavior characterized by specific lengths scales. Here, we elaborate a Floquet-based homogenization valid for arbitrary periodically heterogeneous fiber bundles with fibers subject to mutual interactions. This approach allows us to separately evaluate the energy distribution within the fibers and the matrix, and to define an efficiency function able to optimize the mechanical response of the bundle. We show the existence of a characteristic length scale that maximizes the transfer of the elastic energy from the fibers to the matrix, thus reducing the fibers solicitation and enhancing the overall mechanical response. This theory is able to describe the geometrical features of several biomaterials, such as nacre shell, muscle sarcomere, collagen fibril, and spider silk, in excellent agreement with experimental data. Moreover, it can be used to design bioinspired artificial structures with optimal response.

© 2016 Elsevier Masson SAS. All rights reserved.

1. Introduction

The process of evolution over millions of years has generated a wide range of different natural materials and architectures. Among these, fiber bundle assemblies have outstanding mechanical properties, exhibiting a remarkable balance between stiffness, strength and fracture toughness (Smith et al., 1999; Fratzl and Weinkamer, 2007; Meyers et al., 2008; Ashby et al., 1995; Gibson et al., 1995; Ji and Gao, 2004). Such performances are attributed to their peculiar heterogeneous and hierarchical microstructure, with organizations ranging from the molecular to the macroscopic scale (Gao et al., 2003; Yao et al., 2011; Bosia et al., 2012). The smallest units in such materials are simple fibers embedded in a soft matrix. The most important mechanism at the base of the mechanical behavior is the stress transfer between fibers and matrix, which is mediated by shear interactions. There is an overall consensus on the fact that the above general structure, combined

with the shear mechanism, is definitively beneficial for the mechanical response of biological bundles (Gao et al., 2003; Yao et al., 2011; Bosia et al., 2012; Cranford, 2013). Nacre shells, muscle sarcomeres, collagen fibrils, and spider silks are remarkable examples of such high-performance materials. The architecture of these structures is shown in Fig. 1. The nacre (mother-of-pearl) is composed of blocks of aragonite CaCO_3 and a protein organic phase, assembled in a brick and mortar geometry, see panel (a). The mineral platelets (bricks) are separated by an organic phase matrix (mortar) and a distribution of nanosized mineral bridges can be observed at the platelet-platelet interfaces (Shao et al., 2014; Okumura and de Gennes, 2001; Sun and Bhushan, 2012). Panel (b) shows the muscle and sarcomere structures. The geometry of the sarcomere unit is constituted by interdigitating antiparallel filaments of actin and myosin, the elastic titin filaments and the cross-linker proteins (Kossmann and Huxley, 1961; Tedesco et al., 2010). In this case, the shear among actin and titin-myosin filaments is mediated by the matrix of cross-linker proteins. In this work, we always refer to the passive response of the sarcomere structure, the active behavior being not relevant here. Panel (c) shows the structure of collagen-I, the building block of eye's cornea,

* Corresponding author. Institute of Electronics, Microelectronics and Nanotechnology (IEMN UMR CNRS 8520), 59652 Villeneuve d'Ascq, France.

E-mail address: Stefano.Giordano@iemn.univ-lille1.fr (S. Giordano).

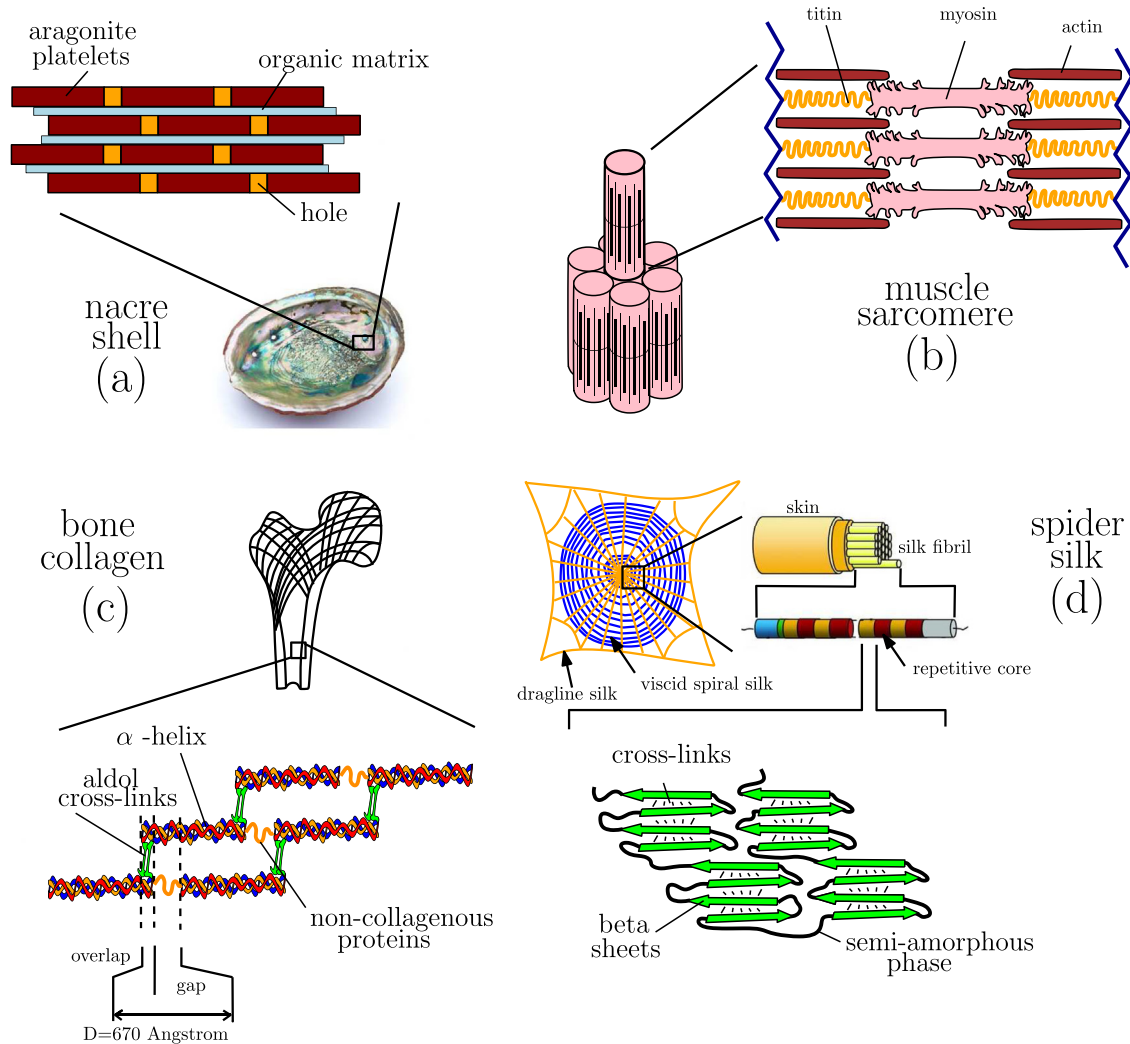


Fig. 1. Architectures of biological materials. Panel (a): bricks-and-mortar structure of nacre (or mother-of-pearl). Panel (b): structure of the muscle fibers based on the sarcomere unit; it is composed of actin, myosin and titin filaments and the cross-linker proteins. Panel (c): collagen structure and schematic representation of the axial arrangement of molecules showing a periodic nanomorphological heterogeneity. Panel (d): schematic orb-web built by a spider composed of fibers with a skin-core structure. We can observe the composition of a silk core fibril: proteins contain highly oriented alanine-rich nanocrystals of antiparallel beta-sheets along the fiber axis embedded in a glycine-rich matrix of random polypeptide chains and moderately oriented helical structures (adapted from [Huang et al., 2012](#), with permission).

skin, tendon and bone. Tropocollagen molecules (length ~ 300 nm) are assembled in fibrils (length $\sim 1\mu\text{m}$), which arrange to form the collagen fiber (length $\sim 10\mu\text{m}$) ([Holmes et al., 2001](#); [Jäger and Fratzl, 2000](#); [Hulmes et al., 1995](#)). Here, the shear transfer between fibers is supported by the aldol cross-links. Finally, panel (d) shows the scheme of the spider silk structure. One can find an orb-web built by a spider and its architecture going from the skin-core structure to the organization of the repetitive core ([Huang et al., 2012](#); [Cranford et al., 2012](#)). This core exhibits the typical brick and mortar geometry composed of beta-sheets and a semi-amorphous phase. These examples share three important features: (a) the physical heterogeneity, (b) the geometrical periodicity, and (c) the stress-transfer mechanism between fibers and matrix of the bundle. These features represent the starting point of the theory here developed.

From the theoretical point of view, several investigations have been conducted in bundle systems. One of the most important paradigm is the classical “shear-lag” interaction scheme among fibers. Originally introduced to study the elasticity and the strength of paper and other fibrous structures ([Cox, 1952](#)), the shear-lag

model was after exploited to understand the behavior of composite materials ([Hutchinson and Jensen, 1990](#); [Nairn, 1997](#)), and to analyse failure phenomena through the well-known fiber bundle model (FBM) ([Pradhan et al., 2010](#); [Kawamura et al., 2012](#)). Initially introduced for studying the failure of spun cotton yarns ([Peirce, 1926](#)), the FBM was further elaborated for considering a parallel arrangement of fibers with statistically distributed strength ([Daniels, 1945](#)). In the FBM context, the shear-lag model has been largely adopted to study the matrix power-law creep compliance ([Lagoudas et al., 1989](#); [Beyerlein et al., 1998](#); [Mahesh and Phoenix, 2004](#)), the nonlinear matrix ([Mason et al., 1992](#)) and the matrix plasticity ([Beyerlein and Phoenix, 1996](#)). Further, the shear-lag model has been recently used to investigate the effects of a population of cracks on the overall mechanical bundle behavior ([Manca et al., 2014a, 2015](#)). The matrix-fibers interaction, based on the shear-lag paradigm, has been shown to yield a spatially non-local elasticity with a size-dependent behavior ([Wada and Tanaka, 2011](#)). This behavior is at the origin of optimal length scales controlling both the fiber length and their overlapping in the bundle macrostructure ([Buehler, 2006, 2008](#); [Chen et al., 2009](#); [Wei et al.,](#)

2012; Ni et al., 2015). Also, several models have been developed for describing the mechanical behavior of bio-inspired short fiber unidirectional nanocomposites (e.g., composed of carbon nanotubes). In particular, the strength and failure properties (Sun et al., 2015; Zhang et al., 2010, 2014), the effects of the distribution of fibers (Lei et al., 2012) and the elastic bounds of the effective Young's modulus have been thoroughly studied (Lei et al., 2013). While the classical analysis of composites with aligned fibers (Gibson, 2012) and the topical results above reported allowed a crucial understanding of the shear-load mechanism, these techniques are not specifically developed to analyse and optimize arbitrarily complex structures from the point of view of the elastic response and of the energetic balance. Moreover, the actual periodicity of these structures has not been taken into account as basis of the mechanical modeling.

In this work, we develop a theory for homogenizing and optimizing periodically heterogeneous bundle geometries. This theory allows to describe a bundle composed of M fibers arbitrarily distributed on the bundle cross-section, with a periodic arrangement along the longitudinal direction. Therefore, a periodic cell can be always identified. In order to develop a general theory, this cell will be considered as composed of S sub-sections with homogeneous physical properties (Young's moduli of fibers and shear interaction coefficients among fibers). While the geometry of the system is fully three-dimensional, the elastic fields (stress, strain and displacement) are functions of one variable only (the abscissa on the longitudinal direction). To develop our theory, we need to evaluate the effective elastic response of such a periodic bundle structure. In this regard, the classical homogenization schemes allow to determine the effective elastic response of several two- and three-dimensional composite structures (Milton, 2002; Torquato, 2002; Kanaun and Levin, 2008a, 2008b), ranging from dispersions of particles (Walpole, 1981; Kachanov and Sevostianov, 2005; Giordano, 2003, 2005; Colombo and Giordano, 2011) to distributions of cracks (Kachanov, 1992, 1994; Giordano and Colombo, 2007a; Giordano and Colombo, 2007b). However, these classical approaches are not appropriate to determine the effective stiffness of periodically inhomogeneous shear-lag bundles, which are essentially one-dimensional systems. Therefore, we propose here a Floquet-based homogenization, yielding an exact closed-form expression for the overall Young's modulus of the bundle. In addition, this analysis allows the determination of the elastic energy accumulated within the fibers (under extension) and within the matrix (under shear). The knowledge of these energies allows to define a suitable efficiency function \mathcal{E} , used to optimize the bundle structure. The underlying idea is that the elastic response is optimized by transferring, as much as possible, the energy from the fibers to the matrix. Indeed, in consistency with the Griffith (1920) or Irwin (1957) criterion for crack growth, minimizing the elastic energy stored in the fibers reduces the possibility of creation and propagation of fractures. On the other hand, the consequently stronger sollicitation of the matrix is less critical since it is typically composed of a soft material, less subjected to fracture processes. The introduction of the efficiency function \mathcal{E} represents the most important and innovative point of the present development with respect to previous achievements (see, e.g., Gibson, 2012, and papers quoted above). Indeed, it allows us to properly optimize the mechanical response of a bundle (in terms of elastic energy distribution), by fully taking into account the arbitrary periodicity and heterogeneity of the system. Importantly, if we study the shape of \mathcal{E} versus some characteristic lengths of the bundle for quite different fiber-bundle materials, we always observe a maximum corresponding to the optimal structure. Therefore, the maximization of the efficiency function controls the emergency of optimal length scales for fiber bundles. The corresponding results have been

accurately confirmed against available experimental data concerning several biological structures. They can be applied to design optimal bioinspired artificial structure, as well. We remark that our approach is based on a linear elastic model, hence based on linear elastic properties of fibers and matrix. This is an approximation since the matrix of natural bundles may undergo large deformations, thus originating nonlinear behaviors and plastic phenomena (Chen et al., 2009). On the other hand, this approximation allows us to propose an analytical solvable model, capable of considering an arbitrary geometry.

The structure of the paper is the following. In Section 2, we introduce the Floquet-based homogenization theory dealing with an arbitrary bundle geometry. Then, in Section 3, we present the energetic analysis of the system. In Section 4, we analyse an illustrative example of bundle structure by introducing the optimization of the shear efficiency. In Section 5, we show the results concerning more complex structures: the periodic staggered geometry and the staircase geometry. Finally, in Section 6, we discuss how our optimality criterion is able to predict the characteristic lengths of several biological architectures.

2. Effective Young's modulus for arbitrary bundle structures

To begin, we take into consideration a single elastic fiber with cross-section of area Σ . The longitudinal deformation of this one-dimensional system is described by the longitudinal displacement $u(x)$ and the scalar stress $t(x)$, where x is the linear abscissa along the fiber. It means that we consider u and t approximately constant over the cross-section, thus neglecting the dependence on y and z (it is reasonable when $l \gg \sqrt{\Sigma}$). As customarily, after a deformation, the point originally located at x , assumes the new position $x+u(x)$. If we consider a small fiber segment of length dx located at x , we can write the static balance of forces as $F(x)+G(x)\Sigma dx=0$, where $F(x)=t(x+dx)\Sigma-t(x)\Sigma$ is the force applied by the remaining parts of the fiber (on the left and on the right) and $G(x)$ is the externally applied body force (per unit of volume). By dividing the above balance equation by Σdx and performing the limit for $dx \rightarrow 0$, we obtain the equation

$$\frac{\partial t(x)}{\partial x} + G(x) = 0. \quad (1)$$

Moreover, we have to introduce the constitutive equation for the elasticity of the fiber. To do this, we consider a linear relationship (Hooke law) between the scalar stress and the scalar strain $\varepsilon(x)=\partial u(x)/\partial x$, as follows

$$t(x) = E\varepsilon(x) = E \frac{\partial u(x)}{\partial x}, \quad (2)$$

where E is the Young's modulus of the fiber.

Let us now consider a bundle of M fibers, which are parallel but arbitrarily arranged on the perpendicular plane (cross-section of the bundle). Accordingly to previous analysis for one fiber, the system is described by the following set of equations

$$\frac{\partial t_i(x)}{\partial x} = -G_i(x), \quad (3)$$

$$\frac{\partial u_i(x)}{\partial x} = \frac{1}{E_i(x)} t_i(x), \quad (4)$$

for $\forall i = 1, \dots, M$, where the force applied to each fiber is given by

$$G_i(x) = \sum_{j=1}^M k_{ij}(x) [u_j(x) - u_i(x)], \quad (5)$$

describing the linear interaction among the fibers within the bundle. For the sake of generality, in this scheme we considered both the Young's moduli E_i and the interaction coefficients k_{ij} as functions of the abscissa x (heterogeneous system). In particular, this is useful to introduce a bundle structure characterized by a spatial period L . We suppose that each cell of periodicity is composed of S homogeneous bundle segments having lengths l_n ($n=1, \dots, S$) with $\sum_{n=1}^S l_n = L$ (see Fig. 2). Moreover, we consider all fibers with the same uniform cross-section Σ . For any homogeneous segment of the cell, we can write the elastostatic stress-displacement interaction equations

$$\frac{dt_i}{dx} = -\sum_{j=1}^M k_{ij}^{(n)} (u_j - u_i), \quad (6)$$

$$\frac{du_i}{dx} = \frac{1}{E_i^{(n)}} t_i, \quad (7)$$

where $t_i(x)$ and $u_i(x)$ are longitudinal stress and displacement along the i -th fiber, $k_{ij}^{(n)}$ are the interaction coefficients and $E_i^{(n)}$ represent the Young's moduli of the M fibers within the n -th segment ($i, j=1, \dots, M$ and $n=1, \dots, S$). It means that we have $k_{ij}(x) = k_{ij}^{(1)}$ and $E_i(x) = E_i^{(1)}$ in the first segment ($0 < x < l_1$), $k_{ij}(x) = k_{ij}^{(2)}$ and $E_i(x) = E_i^{(2)}$ in the second segment ($l_1 < x < l_1 + l_2$), and so forth. Therefore $k_{ij}(x)$ and $E_i(x)$ are piece-wise periodic function of x with period L . While Eq. (6) represents the balance of forces for each fiber, Eq. (7) describes the linear response controlled by the Young's modulus E_i . The sum in the right hand side of Eq. (6) means that when $u_j \neq u_i$ a force $-k_{ij}^{(n)}(u_j - u_i)$ is applied to the i -th fibre and a force $k_{ij}^{(n)}(u_j - u_i)$ is applied to the j -th fiber (see the works by Manca et al., 2014a, 2015, for further details). The symmetrical matrix $k_{ij}^{(n)}$ ($k_{ij}^{(n)} = k_{ji}^{(n)}$ with $k_{ii}^{(n)} = 0$) is straightforwardly associated to the (arbitrary) graph describing the fiber interactions on the cross-section of the bundle. Of course, being the values of $E_i^{(n)}$ and $k_{ij}^{(n)}$ n -dependent (i.e. segment-dependent), we generate the arbitrary physical heterogeneity within the system. For any segment we introduce the following matrix representation of the previous balance equations

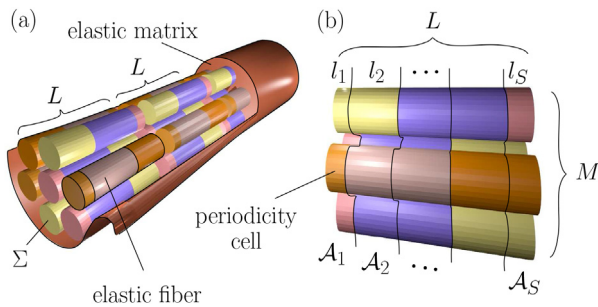


Fig. 2. (a) Scheme of a periodic bundle composed of M piece-wise homogeneous fibers embedded in an elastic matrix. (b) Structure of a periodic cell composed of S segments of lengths l_1, \dots, l_S (with $\sum_{n=1}^S l_n = L$). Each segment is described by a matrix \mathcal{A}_n containing all Young's moduli and interaction coefficients.

$$\frac{d\vec{\xi}}{dx} = \mathcal{A}_n \vec{\xi} \quad \forall n = 1, \dots, S, \quad (8)$$

where $\vec{\xi} = (t_1, u_1, t_2, u_2, \dots)^T \in \mathbb{R}^{2M}$ represents the state vector of the system (T means transposed) and \mathcal{A}_n characterizes the mechanics of the n -th segment

$$\mathcal{A}_n = \begin{pmatrix} 0 & \sum_j k_{1j}^{(n)} & 0 & -k_{12}^{(n)} & \dots & 0 & -k_{1M}^{(n)} \\ \frac{1}{E_1^{(n)}} & 0 & 0 & 0 & \dots & 0 & 0 \\ 0 & -k_{21}^{(n)} & 0 & \sum_j k_{2j}^{(n)} & \dots & 0 & -k_{2M}^{(n)} \\ \vdots & \vdots & \vdots & \vdots & \ddots & \vdots & \vdots \\ 0 & -k_{M1}^{(n)} & 0 & -k_{M2}^{(n)} & \dots & 0 & \sum_j k_{Mj}^{(n)} \\ 0 & 0 & 0 & 0 & \dots & \frac{1}{E_M^{(n)}} & 0 \end{pmatrix}. \quad (9)$$

Finally, we have S linear differential systems for the S segments of the periodic cell ($n=1, \dots, S$). Moreover, it is important to remark that the state vector $\vec{\xi}$, being composed of stresses and displacements, must be continuous at any segment interface. It means that we consider ideal mechanical contacts between adjacent segments. We can further observe that, globally, we are dealing with a Floquet system of the following form

$$\frac{d\vec{\xi}}{dx} = \mathcal{A}(x) \vec{\xi}, \quad (10)$$

which is valid for the entire bundle, where $\mathcal{A}(x) = \mathcal{A}(x+L)$ being $L = \sum_{n=1}^S l_n$ the period of the structure. In particular, we have $\mathcal{A}(x) = \mathcal{A}_1$ in the first segment ($0 < x < l_1$), $\mathcal{A}(x) = \mathcal{A}_2$ in the second segment ($l_1 < x < l_1 + l_2$), and so forth.

We are interested in defining and calculating the effective Young's modulus of the structure. To do this, we can imagine an overall displacement field formed by a linear term describing the uniform prescribed strain, plus an additional perturbation due to the relaxation of the heterogeneous structure (shear among fibers induced by the inhomogeneity)

$$u_i(x) = \varepsilon x + \delta_i(x), \quad (11)$$

where ε is the prescribed strain and δ_i is the local perturbation generated by shear interaction effects. We remark that, although the prescribed strain is uniform, the actual strain in each fiber is not uniform because of the heterogeneity of the bundle and the interactions among fibers. This point is taken into account by the unknown functions $\delta_i(x)$, which, in general, are not linear and can be calculated as described below. The final lengths of all fibers in the cell must be the same after the relaxation (all fibers must cover the whole real axis subdivided in periodic cells). Therefore, the perturbations $\delta_i(x)$ are periodic functions of period L . We can also define the following quantity

$$\vec{\xi} = \vec{\eta} + \varepsilon x \vec{v}, \quad (12)$$

where $\vec{\eta} = (t_1, \delta_1, t_2, \delta_2, \dots)^T$ and $\vec{v} = (0, 1, 0, 1, \dots)^T$. Hence, we

can write

$$\frac{d\vec{\eta}}{dx} = \frac{d\vec{\xi}}{dx} - \varepsilon \vec{v} = \mathcal{A}(x)\vec{\xi} - \varepsilon \vec{v}, \quad (13)$$

or, equivalently

$$\frac{d\vec{\eta}}{dx} = \mathcal{A}(x)\vec{\eta} + \varepsilon[\mathcal{A}(x)\mathcal{X} - \mathcal{I}_{2M}]\vec{v}, \quad (14)$$

where \mathcal{I}_{2M} is the identity matrix of order $2M$. Now, if we observe the structure of the matrix in Eq. (9), we note that the relation $\mathcal{A}(x)\vec{v} = 0$ is always verified in each segment of the structure (i.e. $\forall x$), and therefore we obtain

$$\frac{d\vec{\eta}}{dx} = \mathcal{A}(x)\vec{\eta} - \varepsilon \vec{v}. \quad (15)$$

We have seen that the components $\delta_i(x)$ must be periodic; also the $t_i(x)$ must be periodic for the continuity of the stress. Finally, we search for the periodic solutions of Eq. (15). From the mathematical point of view, this is a Floquet system of differential equations with an additional constant term. The fundamental matrix solution of a general Floquet system is defined by $d\Phi(x)/dx = \mathcal{A}(x)\Phi(x)$ with the condition $\Phi(0) = \mathcal{I}_{2M}$. This initial condition can be arbitrarily chosen (nonsingular) (Pontryagin, 1962), and we fixed $\Phi(0) = \mathcal{I}_{2M}$ in order to simplify further calculations, in particular to impose the value $\vec{\eta}(0)$ in the solution of Eq. (15). The fundamental matrix can be always written in the form

$$\Phi(x) = \mathcal{P}(x)\exp(\mathcal{B}x), \quad (16)$$

where $\mathcal{P}(x)$ is a periodic matrix and \mathcal{B} a constant one (Floquet-Lyapunov theorem, see Pontryagin, 1962). Here, we also consider the relation $\mathcal{P}(0) = \mathcal{P}(L) = \mathcal{I}_{2M}$ coming from the fact that $\Phi(0) = \mathcal{I}_{2M}$. The general solution of Eq. (15) can be written as follows

$$\begin{aligned} \vec{\eta}(x) &= \Phi(x)\vec{\eta}(0) - \int_0^x \Phi(x)\Phi^{-1}(y)\varepsilon \vec{v} dy = \\ &= \mathcal{P}(x)\exp(\mathcal{B}x) \left[\vec{\eta}(0) - \int_0^x \exp(-\mathcal{B}y)\mathcal{P}^{-1}(y)\varepsilon \vec{v} dy \right]. \end{aligned} \quad (17)$$

In particular, we have

$$\vec{\eta}(L) = \mathcal{P}(L)\exp(\mathcal{B}L) \left[\vec{\eta}(0) - \int_0^L \exp(-\mathcal{B}y)\mathcal{P}^{-1}(y)\varepsilon \vec{v} dy \right], \quad (18)$$

where we have substituted $x=L$. Now, we search for a periodic solution for $\vec{\eta}$ and, therefore, we impose $\vec{\eta}(L) = \vec{\eta}(0)$, by obtaining

$$[\mathcal{I}_{2M} - \exp(-\mathcal{B}L)]\vec{\eta}(0) = \int_0^L \exp(-\mathcal{B}y)\mathcal{P}^{-1}(y)\varepsilon \vec{v} dy, \quad (19)$$

where we used the condition $\mathcal{P}(L) = \mathcal{I}_{2M}$.

It is important to observe that the problem defined in Eq. (19) for obtaining $\vec{\eta}(0)$ has multiple solutions for the following reasons: firstly, we have imposed an overall strain to the periodic bundle structure and therefore we can imagine an arbitrary displacement to the whole system, thus generating an infinity of

solutions. It means that we can add the same constant to all functions $\delta_i(x)$ without changing the strain and stress fields within the bundle. Moreover, according to the interaction scheme between the fibers, we can always divide the entire bundle in a number r of sub-bundles not connected by any interaction ($1 \leq r \leq M$). In this case, we will have r degrees of freedom for the arbitrary displacements and, therefore, the rank of the matrix $\mathcal{I}_{2M} - \exp(-\mathcal{B}L)$ will be $2M-r$. Even for the simple case of a completely connected bundle ($r=1$), we will have a matrix $\mathcal{I}_{2M} - \exp(-\mathcal{B}L)$ without full rank, being in this case $2M-1$.

Anyway, the translations of the independent sub-bundles are not relevant for the overall mechanical behavior of the system. Hence, for obtaining a solution for $\vec{\eta}(0)$ from Eq. (19) we will use the Moore-Penrose pseudo-inverse, in order to solve the problem of the reduced rank (Moore, 1920; Penrose, 1955). The Moore-Penrose pseudo-inverse \mathcal{N}^+ (n by m) of a matrix \mathcal{N} (m by n) is defined by the four properties $\mathcal{N}\mathcal{N}^+\mathcal{N} = \mathcal{N}$, $\mathcal{N}^+\mathcal{N}\mathcal{N}^+ = \mathcal{N}^+$, $(\mathcal{N}\mathcal{N}^+)^* = \mathcal{N}\mathcal{N}^+$, and $(\mathcal{N}^+\mathcal{N})^* = \mathcal{N}^+\mathcal{N}$, where the symbol \mathcal{M}^* indicates the conjugate transposed of the matrix \mathcal{M} . By means of this definition, \mathcal{N}^+ always exists and it is unique (Ben-Israel and Greville, 2003; Golub and Van Loan, 1996). It is possible to prove that given an arbitrary system $\mathcal{N}\vec{q} = \vec{b}$ ($\vec{q} \in \mathbb{R}^n$, $\vec{b} \in \mathbb{R}^m$), it has at least a solution for \vec{q} if and only if $\mathcal{N}\mathcal{N}^+\vec{b} = \vec{b}$ (Ben-Israel and Greville, 2003; Golub and Van Loan, 1996). In this case the general solution is given by $\vec{q} = \mathcal{N}^+\vec{b} + (\mathcal{I}_n - \mathcal{N}^+\mathcal{N})\vec{p}$ for any $\vec{p} \in \mathbb{R}^n$ (Ben-Israel and Greville, 2003; Golub and Van Loan, 1996). For our purposes, an arbitrary solution is sufficient since any set of free displacements does not affect the overall mechanical response and, therefore, we will adopt the simpler form $\vec{q} = \mathcal{N}^+\vec{b}$. From Eq. (19), we can finally obtain

$$\vec{\eta}(0) = [\mathcal{I}_{2M} - \exp(-\mathcal{B}L)]^+ \int_0^L \exp(-\mathcal{B}y)\mathcal{P}^{-1}(y)\varepsilon \vec{v} dy, \quad (20)$$

which represents the initial condition corresponding to the periodic solution of Eq. (15). The effective Young's modulus of the overall structure can be defined by

$$E_{eff} = \frac{1}{\varepsilon} \sum_{i=1}^M t_i(0). \quad (21)$$

If we take into account Eq. (6), by summing all equations and exploiting the symmetry of $k_{ij}^{(n)}$, we can easily prove that $\frac{d}{dx} \sum_{i=1}^M t_i(x) = 0$ and, therefore, we can calculate the total stress at any point of the bundle. Hence, in Eq. (21) we calculated the total stress at $x=0$, for the sake of simplicity. In this definition we consider the effective Young's modulus of a single fiber (with section Σ) equivalent to the M -fibers bundle. It means that if we consider M identical and homogeneous fibers with Young's modulus E_f , our definition of the effective modulus yields $E_{eff} = ME_f$. This value exactly corresponds to the Voigt stiffness upper limit.

If we define the vector $\vec{w} = (1, 0, 1, 0, \dots)^T$, we have $\sum_{i=1}^M t_i(0) = \vec{w}^T \vec{\eta}(0)$ and $E_{eff} = \vec{w}^T \vec{\eta}(0) / \varepsilon$. Then, we have proved that the overall Young's modulus is given by the bilinear form

$$E_{eff} = \vec{w}^T \Omega \vec{v}, \quad (22)$$

where

$$\Omega = [\mathcal{A}_{2M} - \exp(-\mathcal{B}L)]^+ \int_0^L \exp(-\mathcal{B}y) \mathcal{P}^{-1}(y) dy. \quad (23)$$

This result is always valid, also in the case of a continuously periodic fiber bundle. Of course, in this case, the couple of matrices \mathcal{B} and \mathcal{P} depends on \mathcal{A} and it should be found by solving the Floquet problem, which is a not simple task from both the theoretical and computational points of view. In the case of a piece-wise bundle structure, as described at the beginning of this section, we can strongly simplify the calculation of E_{eff} . To begin, we observe that the integral $\int_0^L \exp(-\mathcal{B}y) \mathcal{P}^{-1}(y) dy$ in Eq. (23) corresponds to $\int_0^L \Phi^{-1}(y) dy$. Since

$$\Phi^{-1}(y) = \begin{cases} e^{-\mathcal{A}_1 y} & \text{if } 0 < y < l_1 \\ e^{-\mathcal{A}_1 l_1} e^{-\mathcal{A}_2 (y-l_1)} & \text{if } l_1 < y < l_1 + l_2 \\ e^{-\mathcal{A}_1 l_1} e^{-\mathcal{A}_2 l_2} e^{-\mathcal{A}_3 (y-l_1-l_2)} & \text{if } l_1 + l_2 < y < l_1 + l_2 + l_3 \\ \dots & \dots \end{cases}, \quad (24)$$

the integral can be developed as follows

$$\int_0^L \Phi^{-1}(y) dy = \int_0^{l_1} e^{-\mathcal{A}_1 y} dy + e^{-\mathcal{A}_1 l_1} \int_0^{l_2} e^{-\mathcal{A}_2 y} dy + e^{-\mathcal{A}_1 l_1} e^{-\mathcal{A}_2 l_2} \int_0^{l_3} e^{-\mathcal{A}_3 y} dy + \dots, \quad (25)$$

and we get the compact expression

$$\int_0^L \Phi^{-1}(y) dy = \sum_{q=1}^S \left(\prod_{r=1}^{q-1} (\Delta) e^{-\mathcal{A}_r l_r} \right) \int_0^{l_q} e^{-\mathcal{A}_q y} dy, \quad (26)$$

which will be used in the following. The symbol (Δ) means that the product must be ordered with respect to increasing values of r . We will also use the symbol (∇) to intend a decreasing order of the product factors. Now, we introduce a general property useful to calculate $\int_0^{l_q} e^{-\mathcal{A}_q y} dy$, appearing in Eq. (26). As a matter of fact, the result of this integral can be written in a simple explicit closed form only if \mathcal{A}_q is non singular. In our case, we need an expression valid also for a singular \mathcal{A}_q . Hence, we define a matrix \mathcal{E}_q ($4M$ by $4M$), as follows

$$\mathcal{E}_q = \begin{pmatrix} -\mathcal{A}_q & \mathcal{I}_{2M} \\ \mathcal{O}_{2M} & \mathcal{O}_{2M} \end{pmatrix}, \quad (27)$$

where \mathcal{O}_n is the null matrix of order n . We can state that

$$e^{\mathcal{E}_q l_q} = \begin{pmatrix} e^{-\mathcal{A}_q l_q} & \int_0^{l_q} e^{-\mathcal{A}_q y} dy \\ \mathcal{O}_{2M} & \mathcal{I}_{2M} \end{pmatrix}, \quad (28)$$

for any matrix \mathcal{A}_q . To give the proof of this property we can consider the differential system $\vec{x}' = \mathcal{E}_q \vec{x}$, with $\vec{x} \in \mathbb{R}^{4M}$. By solving the system, it is possible to identify the exponential matrix in Eq. (28). Anyway, Eq. (28) allows us to calculate the integral $\int_0^{l_q} e^{-\mathcal{A}_q y} dy$ ($\forall \mathcal{A}_q$) by evaluating a single matrix exponential $e^{\mathcal{E}_q l_q}$ and by extracting the corresponding block. Even more importantly,

this procedure permits to directly evaluate the integral in the left hand side of Eq. (26). Indeed, we can analyse the product of all exponential terms $e^{\mathcal{E}_q l_q}$; if we consider the first two factors, then we have

$$= \begin{pmatrix} e^{\mathcal{E}_1 l_1} e^{\mathcal{E}_2 l_2} \\ e^{-\mathcal{A}_1 l_1} & \int_0^{l_1} e^{-\mathcal{A}_1 y} dy \\ \mathcal{O}_{2M} & \mathcal{I}_{2M} \end{pmatrix} \begin{pmatrix} e^{-\mathcal{A}_2 l_2} & \int_0^{l_2} e^{-\mathcal{A}_2 y} dy \\ \mathcal{O}_{2M} & \mathcal{I}_{2M} \end{pmatrix} \quad (29)$$

$$= \begin{pmatrix} e^{-\mathcal{A}_1 l_1} e^{-\mathcal{A}_2 l_2} & e^{-\mathcal{A}_1 l_1} \int_0^{l_2} e^{-\mathcal{A}_2 y} dy + \int_0^{l_1} e^{-\mathcal{A}_1 y} dy \\ \mathcal{O}_{2M} & \mathcal{I}_{2M} \end{pmatrix}.$$

If we continue to multiply all terms, we eventually obtain

$$\prod_{q=1}^S (\Delta) e^{\mathcal{E}_q l_q} = \begin{pmatrix} \prod_{q=1}^S (\Delta) e^{-\mathcal{A}_q l_q} & \int_0^L \Phi^{-1}(y) dy \\ \mathcal{O}_{2M} & \mathcal{I}_{2M} \end{pmatrix}, \quad (30)$$

where we used Eq. (26). It means that the product of all exponential terms $e^{\mathcal{E}_q l_q}$ immediately furnishes, in its second block, the integral in Eq. (26). Moreover, also the first block in Eq. (30) is important to evaluate the effective Young's modulus of the heterogeneous bundle. For a Floquet system $\frac{d\vec{\eta}}{dx} = \mathcal{A}(x) \vec{\eta}$, we have the solution $\vec{\eta}(x) = \mathcal{P}(x) e^{\mathcal{B}x} \vec{\eta}(0)$. On the other hand, if $\mathcal{A}(x)$ is periodic piece-wise constant we also have $\vec{\eta}(x) = e^{\mathcal{A}_p l_p} \dots e^{\mathcal{A}_1 l_1} \vec{\eta}(0)$ when $x = l_1 + \dots + l_p$ ($x \leq L, p \leq S$). By comparing the two solutions for $x=L$, and by using the property $\mathcal{P}(L) = \mathcal{I}_{2M}$, we immediately obtain $e^{\mathcal{B}L} = e^{\mathcal{A}_S l_S} \dots e^{\mathcal{A}_1 l_1}$. Hence, Eq. (30) can be rewritten as

$$\prod_{q=1}^S (\Delta) e^{\mathcal{E}_q l_q} = \begin{pmatrix} e^{-\mathcal{B}L} & \int_0^L \Phi^{-1}(y) dy \\ \mathcal{O}_{2M} & \mathcal{I}_{2M} \end{pmatrix}. \quad (31)$$

So, in the structure of $\prod_{q=1}^S (\Delta) e^{\mathcal{E}_q l_q}$ we have the two main ingredients to compute E_{eff} through Eqs. (22) and (23). We finally proved the following:

Theorem 1. *Given the heterogeneous bundle composed of M fibers and S segments, described by matrices \mathcal{A}_q and lengths l_q , we can define*

$$\mathcal{E}_q = \begin{pmatrix} -\mathcal{A}_q & \mathcal{I}_{2M} \\ \mathcal{O}_{2M} & \mathcal{O}_{2M} \end{pmatrix}, \quad \prod_{q=1}^S (\Delta) e^{\mathcal{E}_q l_q} = \begin{pmatrix} \mathcal{D} & \varepsilon \\ \mathcal{O}_{2M} & \mathcal{I}_{2M} \end{pmatrix}. \quad (32)$$

Then, the effective Young's modulus is determined by the following bilinear form

$$E_{eff} = \vec{w}^T \Omega \vec{v} = \vec{w}^T (\mathcal{I}_{2M} - \mathcal{D})^+ \varepsilon \vec{v}, \quad (33)$$

where $\Omega = (\mathcal{I}_{2M} - \mathcal{D})^+ \varepsilon$, $\vec{v} = (0, 1, 0, 1, \dots)^T$ and $\vec{w} = (1, 0, 1, 0, \dots)^T$.

This theorem gives the complete theoretical assessment of the fiber bundle elastic behavior and allows an efficient numerical computation of the effective Young's modulus for an arbitrary structure.

3. Energetic considerations

In this Section, we introduce the definitions of the elastic energy

adsorbed in the fibers of the bundle, and in the matrix controlling the shear interactions among them. For convenience, we take into consideration a periodic cell and we calculate the average energy density of both contributions. The average energy density stored in the fibers can be defined as

$$w_f = \sum_{i=1}^M \int_0^L \frac{t_i(x)\varepsilon_i(x)}{2L} dx = \sum_{i=1}^M \int_0^L \frac{E_i(x)t_i^2(x)}{2L} dx, \quad (34)$$

where $\varepsilon_i = du_i/dx$ and $t_i = E_i\varepsilon_i$. On the other hand, the average energy density stored in the matrix can be introduced through the expression

$$w_m = \frac{1}{2} \sum_{i=1}^M \sum_{j=1}^M \frac{1}{L} \int_0^L \frac{1}{2} k_{ij}(x) [u_i(x) - u_j(x)]^2 dx, \quad (35)$$

where the term $\frac{1}{2}k_{ij}(x)[u_i(x) - u_j(x)]^2$ represents the spring-like contribution of each interaction and the factor 1/2 in front of the sums is necessary to correctly count all the terms (that are considered twice by the double sum). We recall that in Eqs. (34) and (35) the piece-wise constant functions $E_i(x)$ and $k_{ij}(x)$ represent the heterogeneity of the periodic cell generated by the different homogeneous segments, as defined in Section 2. We obtain here explicit expressions for w_f and w_m , which are valid for a periodic heterogeneous fiber bundle.

3.1. Energy density within the fibers

Let us firstly consider the fibers energy contribution and define the diagonal matrix $\varepsilon(x)=\text{diag}(1/E_1(x),0,1/E_2(x),0,\dots)$. Then, Eq. (34) can be rewritten as

$$\begin{aligned} w_f &= \frac{1}{2L} \int_0^L \vec{\xi}^T(x) \mathcal{E}(x) \vec{\xi}(x) dx \\ &= \frac{1}{2L} \int_0^L \vec{\xi}^T(0) \Phi^T(x) \mathcal{E}(x) \Phi(x) \vec{\xi}(0) dx, \end{aligned} \quad (36)$$

where we introduced the solution of Eq. (10). Now, we deduce from Eq. (12) that $\vec{\xi}(0) = \vec{\eta}(0)$ and from Eqs. (20) and (23) that $\vec{\eta}(0) = \varepsilon\Omega\vec{v}$; hence, the energy density of the fibers is

$$w_f = \frac{1}{2L} \varepsilon^2 \vec{v}^T \Omega^T \int_0^L \Phi^T(x) \mathcal{E}(x) \Phi(x) dx \Omega \vec{v}. \quad (37)$$

We propose now an efficient procedure to calculate Eq. (37) and, in particular, the integral $\mathcal{E} = \int_0^L \Phi^T(x) \mathcal{E}(x) \Phi(x) dx$. If we consider a piece-wise homogeneous bundle such an integral can be conveniently developed as follows

$$\begin{aligned} \mathcal{E} &= \int_0^L \Phi^T(x) \mathcal{E}(x) \Phi(x) dx \\ &= \int_0^{l_1} e^{\mathcal{A}_1^T y} \mathcal{E}_1 e^{\mathcal{A}_1 y} dy + e^{\mathcal{A}_1^T l_1} \int_0^{l_2} e^{\mathcal{A}_2^T y} \mathcal{E}_2 e^{\mathcal{A}_2 y} dy e^{\mathcal{A}_1 l_1} \\ &+ e^{\mathcal{A}_1^T l_1} e^{\mathcal{A}_2^T l_2} \int_0^{l_3} e^{\mathcal{A}_3^T y} \mathcal{E}_3 e^{\mathcal{A}_3 y} dy e^{\mathcal{A}_2 l_2} e^{\mathcal{A}_1 l_1} \dots, \end{aligned} \quad (38)$$

where ε_q represents the diagonal matrix $\text{diag}(1/E_1,0,1/E_2,0,\dots)$ composed of the Young's moduli of the q -th segment of the periodic cell. The general form of \mathcal{E} can be written as

$$\mathcal{E} = \sum_{q=1}^S \left(\prod_{r=1}^{q-1} (\Delta) e^{\mathcal{A}_r^T l_r} \right) \int_0^{l_q} e^{\mathcal{A}_q^T y} \mathcal{E}_q e^{\mathcal{A}_q y} dy \left(\prod_{p=1}^{q-1} (\nabla) e^{\mathcal{A}_p l_p} \right), \quad (39)$$

where, as before, the symbols (Δ) and (∇) indicate the order of the products. We need therefore an efficient technique to evaluate the integrals of the form $\int_0^{l_q} e^{\mathcal{A}_q^T y} \mathcal{E}_q e^{\mathcal{A}_q y} dy$ for any matrix \mathcal{A}_q (singular or non singular). We define a matrix \mathcal{D}_q ($4M$ by $4M$) as follows

$$\mathcal{D}_q = \begin{pmatrix} -\mathcal{A}_q^T & \mathcal{E}_q \\ \mathcal{O}_{2M} & \mathcal{A}_q \end{pmatrix}, \quad (40)$$

and we state that

$$e^{\mathcal{D}_q l_q} = \begin{pmatrix} e^{-\mathcal{A}_q^T l_q} & e^{-\mathcal{A}_q^T l_q} \int_0^{l_q} e^{\mathcal{A}_q^T y} \mathcal{E}_q e^{\mathcal{A}_q y} dy \\ \mathcal{O}_{2M} & e^{\mathcal{A}_q l_q} \end{pmatrix}, \quad (41)$$

for any matrix \mathcal{A}_q . As before, to prove this property, we may introduce the differential system $\vec{x}' = \mathcal{D}_q \vec{x}$, with $\vec{x} \in \mathbb{R}^{4M}$. Its solution allows the determination of the exponential matrix in Eq. (41) (other similar relations have been found by Van Loan, 1978).

We show now that this property is useful to directly determine the value of \mathcal{E} . To this aim, let us analyse the product of all exponential terms $e^{\mathcal{D}_q l_q}$, performed in decreasing order. Defining $\mathcal{F}_q = \int_0^{l_q} e^{\mathcal{A}_q^T y} \mathcal{E}_q e^{\mathcal{A}_q y} dy$ and considering the first two factors, we have

$$\begin{aligned} e^{\mathcal{D}_2 l_2} e^{\mathcal{D}_1 l_1} &= \begin{pmatrix} e^{-\mathcal{A}_2^T l_2} & e^{-\mathcal{A}_2^T l_2} \mathcal{F}_2 \\ \mathcal{O}_{2M} & e^{\mathcal{A}_2 l_2} \end{pmatrix} \begin{pmatrix} e^{-\mathcal{A}_1^T l_1} & e^{-\mathcal{A}_1^T l_1} \mathcal{F}_1 \\ \mathcal{O}_{2M} & e^{\mathcal{A}_1 l_1} \end{pmatrix} \\ &= \begin{pmatrix} e^{-\mathcal{A}_2^T l_2} e^{-\mathcal{A}_1^T l_1} & e^{-\mathcal{A}_2^T l_2} e^{-\mathcal{A}_1^T l_1} \mathcal{F}_1 + e^{-\mathcal{A}_2^T l_2} \mathcal{F}_2 e^{\mathcal{A}_1 l_1} \\ \mathcal{O}_{2M} & e^{\mathcal{A}_2 l_2} e^{\mathcal{A}_1 l_1} \end{pmatrix}. \end{aligned} \quad (42)$$

By multiplying all factors, the following compact expression is eventually obtained

$$\prod_{q=1}^S (\nabla) e^{\mathcal{D}_q l_q} = \begin{pmatrix} \prod_{q=1}^S (\nabla) e^{-\mathcal{A}_q^T l_q} & \prod_{q=1}^S (\nabla) e^{-\mathcal{A}_q^T l_q} \mathcal{F}_q \\ \mathcal{O}_{2M} & \prod_{q=1}^S (\nabla) e^{\mathcal{A}_q l_q} \end{pmatrix}, \quad (43)$$

where we exploited Eq. (39). This result can be used to extract the block corresponding to \mathcal{E} and it can be inserted in the final expression for the fibers energy density $w_f = \frac{1}{2L} \varepsilon^2 \vec{v}^T \Omega^T \mathcal{E} \Omega \vec{v}$, see Eq. (37). The whole procedure can be summed up by the following:

Theorem 2. Given the heterogeneous bundle composed of M fibers and S segments, described by matrices \mathcal{A}_q , ε_q and lengths l_q , we can define

$$\mathcal{D}_q = \begin{pmatrix} -\mathcal{A}_q^T & \mathcal{E}_q \\ \mathcal{O}_{2M} & \mathcal{A}_q \end{pmatrix}, \quad \prod_{q=1}^S (\nabla) e^{\mathcal{D}_q l_q} = \begin{pmatrix} \mathcal{R} & \mathcal{I} \\ \mathcal{O}_{2M} & \mathcal{W} \end{pmatrix}. \quad (44)$$

Then, the fibers energy density is determined by the following quadratic form

$$w_f = \frac{1}{2L} \varepsilon^2 \vec{v}^T \Omega^T \mathcal{G} \Omega \vec{v} = \frac{1}{2L} \varepsilon^2 \vec{v}^T \Omega^T \mathcal{R}^{-1} \mathcal{S} \Omega \vec{v} = \frac{1}{2L} \varepsilon^2 \vec{v}^T \Omega^T \mathcal{W}^T \mathcal{S} \Omega \vec{v}, \tag{45}$$

where $\mathcal{G} = \mathcal{R}^{-1} \mathcal{S} = \mathcal{W}^T \mathcal{S}$, $\vec{v} = (0, 1, 0, 1, \dots)^T$ and $\Omega = (\mathcal{S}_{2M} - \mathcal{S})^+ \varepsilon$ (one can see Theorem 1 for the determination of \mathcal{S} and ε). Moreover, the matrix identity $\mathcal{R}^T = \mathcal{W}^{-1} = \mathcal{S}$ is satisfied, where \mathcal{S} is defined in Theorem 1.

3.2. Energy density within the matrix

We analyse now the energy density accumulated in the matrix, i.e. the energy density concerning the interaction among the fibers. Accordingly, we elaborate Eq. (35) as follows

$$w_m = \frac{1}{2L} \sum_{i=1}^M \sum_{j=1}^M \int_0^L [u_i(x) k_{ij}(x) u_i(x) - u_i(x) k_{ij} u_j(x)] dx = \frac{1}{2L} \int_0^L \vec{\xi}^T(x) \mathcal{H}(x) \vec{\xi}(x) dx. \tag{46}$$

where the matrix $\mathcal{H}(x)$ is defined as follows. For any segment of the bundle period we define

$$\mathcal{H}_n = \begin{pmatrix} 0 & 0 & 0 & 0 & \dots & 0 & 0 \\ 0 & \sum_j k_{1j}^{(n)} & 0 & -k_{12}^{(n)} & \dots & 0 & -k_{1M}^{(n)} \\ 0 & 0 & 0 & 0 & \dots & 0 & 0 \\ 0 & -k_{21}^{(n)} & 0 & \sum_j k_{2j}^{(n)} & \dots & 0 & -k_{2M}^{(n)} \\ \vdots & \vdots & \vdots & \vdots & \dots & \vdots & \vdots \\ 0 & -k_{M1}^{(n)} & 0 & -k_{M2}^{(n)} & \dots & 0 & \sum_j k_{Mj}^{(n)} \end{pmatrix}. \tag{47}$$

Then we can introduce the periodical matrix $\mathcal{H}(x) = \mathcal{H}(x + L)$ being $L = \sum_{n=1}^S l_n$ the period of the structure. In particular, we have $\mathcal{H}(x) = \mathcal{H}_1$ in the first segment ($0 < x < l_1$), $\mathcal{H}(x) = \mathcal{H}_2$ in the second segment ($l_1 < x < l_1 + l_2$), and so forth. Since Eq. (46) is formally identical to Eq. (36), the procedure already developed in Section 3.1 can be directly applied to obtain the final result concerning the interaction energy density for an arbitrary bundle structure. The final results can be therefore formulated as follows, in perfect analogy with Theorem 2:

Theorem 3. Given the heterogeneous bundle composed of M fibers and S segments, described by matrices \mathcal{A}_q , \mathcal{H}_q and lengths l_q , we can define

$$\mathcal{C}_q = \begin{pmatrix} -\mathcal{A}_q^T & \mathcal{H}_q \\ \mathcal{C}_{2M} & \mathcal{A}_q \end{pmatrix}, \prod_{q=1}^S (\nabla) e^{\mathcal{C}_q l_q} = \begin{pmatrix} \mathcal{R} & \mathcal{M} \\ \mathcal{C}_{2M} & \mathcal{W} \end{pmatrix}. \tag{48}$$

Then, the matrix energy density (interaction energy) is determined by the following quadratic form

$$w_m = \frac{1}{2L} \varepsilon^2 \vec{v}^T \Omega^T \mathcal{R}^{-1} \mathcal{M} \Omega \vec{v} = \frac{1}{2L} \varepsilon^2 \vec{v}^T \Omega^T \mathcal{W}^T \mathcal{M} \Omega \vec{v}, \tag{49}$$

where $\vec{v} = (0, 1, 0, 1, \dots)^T$ and $\Omega = (\mathcal{S}_{2M} - \mathcal{S})^+ \varepsilon$ (see Theorem 1 for the determination of \mathcal{S} and \mathcal{S}). Also, the matrices \mathcal{R} and \mathcal{S} are the same already introduced in Theorem 2.

To conclude the discussion about the energy balance in the fiber bundle, we prove a general property stating that the energy

accumulated in the homogeneous effective fiber with Young's modulus E_{eff} (see Theorem 1) is identical to the sum of two energy amounts related to fibers (Theorem 2) and matrix (Theorem 3) in the corresponding heterogeneous bundle. This result can be formulated as follows:

Theorem 4. Consider a periodically heterogeneous fiber bundle under an overall strain ε ; then the following relation holds true

$$\frac{1}{2} \varepsilon^2 E_{eff} = w_f + w_m, \tag{50}$$

where the three quantities E_{eff} , w_f and w_m are given in Eqs. respectively. Equivalently, the effective Young's modulus of the composite bundle can be evaluated through the following alternative expressions

$$E_{eff} = \frac{1}{L} \vec{v}^T \Omega^T \mathcal{R}^{-1} (\mathcal{S} + \mathcal{M}) \Omega \vec{v} = \frac{1}{L} \vec{v}^T \Omega^T \mathcal{W}^T (\mathcal{S} + \mathcal{M}) \Omega \vec{v}, \tag{51}$$

where the matrices Ω , \mathcal{R} , \mathcal{W} , \mathcal{S} and \mathcal{M} have been introduced in Theorems 1, 2 and 3.

This result can be seen as a particular version of the Hill-Mandel lemma, typically introduced to study standard composite materials (Qu and Cherkaoui, 2006). In our context, the proof of this property can be done by considering the total energy density $w = w_f + w_m$ for the periodic bundle and by elaborating its expression as follows

$$w = \frac{1}{2L} \sum_{i=1}^M \int_0^L t_i(x) \frac{du_i(x)}{dx} dx + \frac{1}{4L} \sum_{i=1}^M \sum_{j=1}^M \int_0^L k_{ij}(x) [u_i(x) - u_j(x)]^2 dx = \frac{1}{2L} \sum_{i=1}^M [t_i u_i]_0^L - \frac{1}{2L} \sum_{i=1}^M \int_0^L \frac{dt_i(x)}{dx} u_i(x) dx + \frac{1}{4L} \sum_{i=1}^M \sum_{j=1}^M \int_0^L k_{ij}(x) [u_i(x) - u_j(x)]^2 dx, \tag{52}$$

where we have applied an integration by parts in the first integral concerning fibers energy density. Now, we can substitute Eq. (6) to develop the term $dt_i(x)/dx$, by obtaining

$$w = \frac{1}{2L} \sum_{i=1}^M [t_i u_i]_0^L + \frac{1}{2L} \sum_{i=1}^M \int_0^L u_i(x) \sum_{j=1}^M k_{ij} [u_j(x) - u_i(x)] dx + \frac{1}{4L} \sum_{i=1}^M \sum_{j=1}^M \int_0^L k_{ij}(x) [u_i(x) - u_j(x)]^2 dx, \tag{53}$$

where a direct calculation reveals the sum of the two integrals (second and third terms) to be zero. Indeed, we can observe that $\sum_{ij} k_{ij} u_i u_j - \sum_{ij} k_{ij} u_i^2 = -\frac{1}{2} \sum_{ij} k_{ij} u_i^2 - \frac{1}{2} \sum_{ij} k_{ij} u_j^2 + \frac{1}{2} \sum_{ij} 2k_{ij} u_i u_j = -\frac{1}{2} \sum_{ij} k_{ij} (u_i - u_j)^2$. This proves that the integrals cancel out, and we get the simple expression

$$w = \frac{1}{2L} \sum_{i=1}^M [t_i u_i]_0^L = \frac{1}{2L} \sum_{i=1}^M [t_i (\epsilon x + \delta_i)]_0^L \tag{54}$$

where we have introduced Eq. (11), describing the displacement function in a periodic heterogeneous bundle. We can observe that both functions t_i and δ_i are periodic, leading to the relation $[t_i \delta_i]_0^L = t_i(L) \delta_i(L) - t_i(0) \delta_i(0) = 0$. This proves that

$$w = \frac{1}{2L} \sum_{i=1}^M [t_i \epsilon x]_0^L = \frac{\epsilon}{2} \sum_{i=1}^M t_i(L) = \frac{1}{2} \epsilon^2 E_{eff}, \tag{55}$$

where we used the relation $t_i(0)=t_i(L)$ and Eq. (21), defining the effective Young’s modulus of the periodic structure. This concludes the proof of Theorem 4.

4. Analysis of a simple bundle structure: optimization of the shear efficiency

As a simple analytically solvable example, we consider here a system of two parallel fibers ($M=2$), with a periodic cell composed of two sections ($S=2$), as shown in Fig. 3(a). The Young’s moduli E_t and E_b define the elasticity of the fibers, while κ represents their interaction coefficient. It is convenient to introduce the quantities $\lambda = \sqrt{\kappa(1/E_t + 1/E_b)}$ and $p=E_t/E_b$ to compact the notations. This simple structure allow us to perform a complete explicit analysis of the mechanical behavior. To begin, we can consider the response of a single cell subjected to different boundary conditions. Then, we study longer structures (with n cells), and for $n \rightarrow \infty$ we asymptotically reach a periodic system. We will prove that, with an increasing number n , the effects of the boundary conditions progressively diminish, and completely disappear for $n \rightarrow \infty$. Hence, the results obtained for $n \rightarrow \infty$ must be consistent with the theorem proved in Sections 2 and 3, pertinent to periodic systems.

To begin the analysis, we consider a single cell (composed of two segments) subjected to the so-called isometric Helmholtz conditions

$$\begin{cases} u_1(0) = 0 \\ u_2(0) = 0 \end{cases}, \quad \begin{cases} u_1(L) = \delta \\ u_2(L) = \delta \end{cases} \tag{56}$$

prescribing a given displacement on the right end terminals of the fibers by clamping the left end terminals at the origin of the

reference frame. The relation $\vec{\xi}(L) = \exp(\mathcal{A}_2 L) \exp(\mathcal{A}_1 L) \vec{\xi}(0)$, where $\vec{\xi}^T = (t_1, u_1, t_2, u_2)$, combined with Eq. (56) represents a systems of four equations with the four unknowns $t_1(0), t_2(0), t_1(L)$ and $t_2(L)$. $\vec{\xi}(L) = \exp(\mathcal{A}_2 L) \exp(\mathcal{A}_1 L) \vec{\xi}(0)$ (where $L=2\ell$). By solving this system and by defining the Young’s modulus of a single cell under Helmholtz conditions as the total stress divided by the prescribed strain, i.e. $E_{eff,H} = [t_1(L) + t_2(L)]L/\delta$, we eventually obtain the result

$$\frac{E_{eff,H}}{E_b} = \frac{4p(1+p)\lambda\ell}{4p\lambda\ell + (p-1)^2 \tanh(\lambda\ell)} \tag{57}$$

A dual case concerns a single cell subjected to isotensional Gibbs conditions

$$\begin{cases} u_1(0) = 0 \\ u_2(0) = 0 \end{cases}, \quad \begin{cases} t_1(L) = \tau \\ t_2(L) = \tau \end{cases} \tag{58}$$

prescribing a given force applied on the right end terminals of the fibers by clamping the left end terminals at the origin of the reference frame. The relation can be combined with Eq. (58), by yielding a system for the unknowns $t_1(0), t_2(0), u_1(L)$ and $u_2(L)$. In this case, the effective Young’s modulus is defined as the total stress divided by the average strain, $E_{eff,G} = 4\tau L/[u_1(L) + u_2(L)]$, and its final expression can be written as

$$\frac{E_{eff,G}}{E_b} = \frac{4p(1+p)\lambda\ell}{4p\lambda\ell + (p-1) \frac{2\sinh(\lambda\ell)[3 \cosh(\lambda\ell) - 2]}{2 \cosh^2(\lambda\ell) - 1}} \tag{59}$$

We observe that, with different boundary conditions, we have two different effective Young’s moduli for the same structure.

Now, with the aim of going towards a periodic structure, we take into consideration a series of n cells (each composed of two segments as discussed above), and we apply both the Helmholtz and the Gibbs conditions to the whole structure. In this case, the total length is $L=2n\ell$ and the main equation relating the mechanical quantities on the left and right end-terminals is given by $\vec{\xi}(L) = [\exp(\mathcal{A}_2 \ell) \exp(\mathcal{A}_1 \ell)]^n \vec{\xi}(0)$. The definition of the Helmholtz and Gibbs conditions is given, as before, in Eqs. (56) and (58), respectively. Therefore, for the calculation of the effective properties as function of the number of cells n , we have to compute the matrix power $[\exp(\mathcal{A}_2 \ell) \exp(\mathcal{A}_1 \ell)]^n$. Fortunately, the matrix $\exp(\mathcal{A}_2 \ell) \exp(\mathcal{A}_1 \ell)$ can be put in Jordan form with a purely

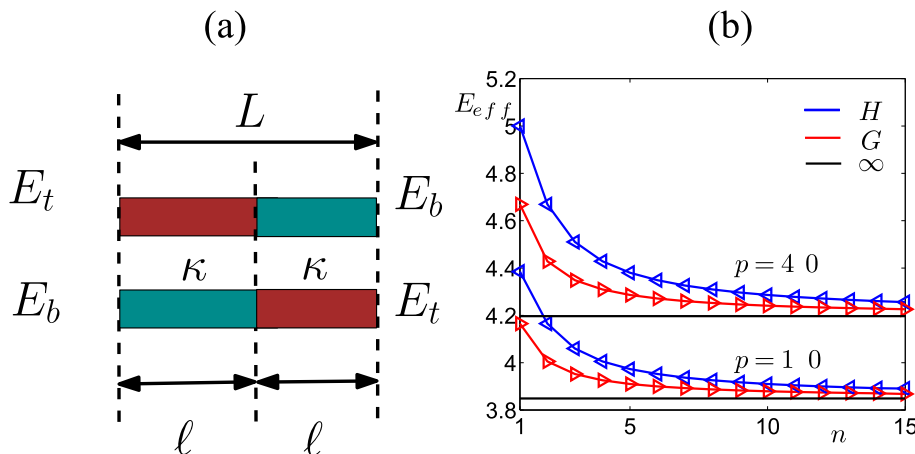


Fig. 3. Panel (a): periodic cell of a simple bundle structure composed of $M=2$ fibers and $S=2$ sections. Panel (b): effective Young’s modulus (in a.u.) of a structure composed of n cells under Helmholtz (H) and Gibbs (G) conditions. For large n , both results converge to the periodic case (∞).

analytical procedure and then we can write $E_{eff,H}(n)$ and $E_{eff,G}(n)$ in closed form. However, the corresponding expressions are rather cumbersome and we do not present here the detailed results for the sake of brevity. The interesting point is that both responses for isometric and isotensional conditions converge, for large n , to the same result

$$\frac{E_{eff,\infty}}{E_b} = \frac{4p(1+p)\lambda\ell}{4p\lambda\ell + 2(p-1)^2 \tanh\left(\frac{\lambda\ell}{2}\right)}, \quad (60)$$

representing the effective Young's modulus of a periodic structure. It is not difficult to prove that this expression is in perfect agreement with Theorem 1, applied to the present case. This behavior can be seen in Fig. 3(b), where we used the following parameters: $\ell=1$, $E_b=1$, $p=10$ and 40 , $\kappa=1$ in a.u. and $\lambda = \sqrt{1+1/p}$. For both values of the contrast p one can observe the convergence to the effective modulus pertinent to the periodic structure. The same behavior can be deduced from Fig. 4, where the effective Young's modulus is represented versus the elastic contrast p for several values of n and for both Helmholtz and Gibbs conditions. It is interesting to note that if we consider $E_t=E_b=E_f$ (i.e. $p=1$) in Eqs. (57) (59) and (60) (Voigt model), we obtain the result $E_{eff,H}=E_{eff,G}=E_{eff,\infty}=2E_f$. This is consistent with the fact that we defined the effective Young's modulus of the system as the Young's modulus of a single fiber (with section Σ) equivalent to the M -fibers bundle (see Section 2). Therefore, in this case the Voigt stiffness upper bound corresponds to $E_{max}=2E_f$. The complicated behaviors represented in Fig. 4 are completely originated by the presence of the shear interactions among fibers. To begin, the augmentation of E_{eff} (H , G or ∞) with increasing x with n fixed can be physically interpreted as follows. If the contrast between E_b and E_t is higher, then we observe a larger difference between the strain induced in the corresponding fibers. This strain difference induces a larger relative displacement between parallel fiber segments, controlled by κ . So, with higher contrast p , we have a stronger effect of the interactions. This causes an increasing of the effective elastic stiffness (also the interactions contribute to the overall stiffness). On the other hand, the decreasing of the effective stiffness with larger values of n (p constant) is related to a different physical mechanism. With given n and p we have a certain relative displacement between parallel fibers. Then, if we consider a system with $n+1$ fibers and the same p , we have a weak effect of the boundary conditions

on the cells and we eventually observe a smaller relative displacement between parallel fibers. Therefore, increasing n , we reduce the effects of the shear interactions. This mechanism finally attenuates the overall elastic stiffness of the bundle.

The terms Helmholtz and Gibbs conditions come from the similar topic concerning the elasticity of flexible and semiflexible polymer chains (Manca et al., 2012a, 2012b, 2013, 2014b). In that case the different responses obtained for finite chains under different boundary conditions are due to statistical mechanics effects (i.e., induced by the temperature). In fact, prescribing different boundary conditions modifies the structure of the phase space and, consequently, alters the calculation of average values of quantities describing the overall elastic response. Only when the thermodynamic limit is achieved (infinite chains), different conditions lead to the same mechanical response (equivalence between statistical ensembles). The situation is conceptually similar for composite bundles (also without temperature effects). Indeed, in this case, the different behavior under different boundary conditions is generated by the relaxation of the internal degrees of freedom (shear effects among the fibers), which is sensible to the quantities prescribed at boundaries (either displacement or stress). As for polymer chains, when we consider an infinite periodic bundle, the elastic response is unique, independently of the fixed conditions. Although, the physical origin of this phenomenon is not exactly the same, it is interesting to underline the analogy between polymer chains and composite bundles.

The behavior of the periodic structure can be obtained not only as limit for $n \rightarrow \infty$ of the system with Helmholtz or Gibbs conditions (or through Theorem 1), but it can be also analysed as follows. We consider a single cell with length $L=2\ell$ and we impose the following boundary conditions, which are able to mimic the behavior of each cell in a periodic structure

$$\begin{cases} u_1(0) = 0 \\ u_1(L) = \delta \end{cases}, \quad \begin{cases} u_2(L) - u_2(0) = \delta \\ t_1(L) = t_1(0) \end{cases}. \quad (61)$$

The first two assumptions impose an average strain $\varepsilon=\delta/L$ to the first fibre; the third condition means that the total elongation of the second fibre must be the same of the first one, allowing, however, possible shear translations between the fibers. Finally, the fourth hypothesis imposes the periodicity of the stress in the first fiber. Please note that the periodicity of the stress in the second one is automatically satisfied since the conservation of the total stress in different bundle sections is a built-in property of the main

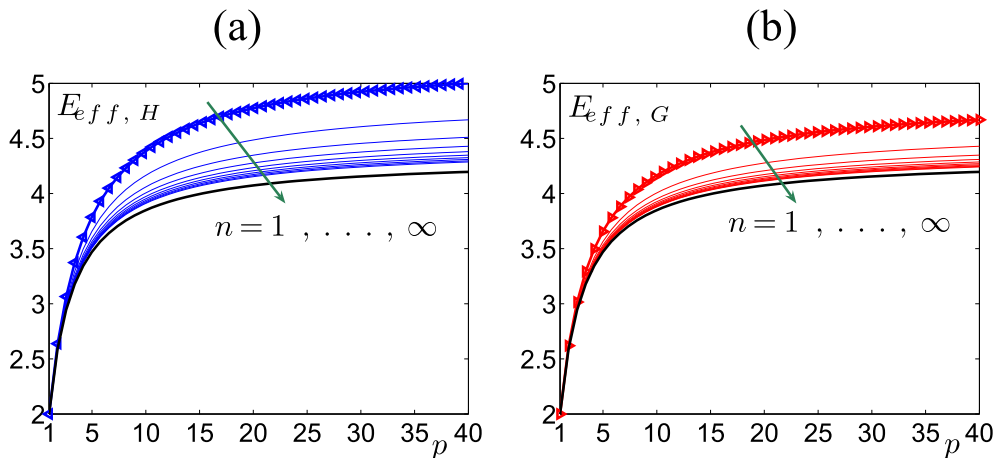


Fig. 4. Effective Young's modulus (in a.u.) of the bundle with Helmholtz conditions (a) and Gibbs conditions (b) versus the elastic contrast p for increasing values of $n=1, \dots, 10$. The curves with triangles correspond to $n=1$, i.e. to Eqs. (57) and (59) and the black solid curves to $n \rightarrow \infty$, i.e. to Eq. (60). We used the same parameters as in Fig. 3(b).

equations of the system (see Eq. (9)). Anyway, by considering Eq. (61) combined with $\vec{\xi}(L) = \exp(\mathcal{A}_2 \ell) \exp(\mathcal{A}_1 \ell) \vec{\xi}(0)$, and by defining the effective Young's modulus as $E_{eff,\infty} = [t_1(L) + t_2(L)]L/\delta$, we can re-obtain Eq. (60), already proved with the limiting process or by Theorem 1. More importantly, the knowledge of the boundary conditions for a single cell of a periodic system allows us to determine the vector $\vec{\xi}(x) \forall x \in (0, L)$. In particular, this result can be used to determine the average energy density stored in the fibers, eventually obtaining

$$\frac{w_f}{E_b} = \frac{1}{2} e^{-2\lambda \ell} \frac{\lambda p(1+p)}{2} \times \frac{2(p-1)^2 \mathcal{F} - \lambda \ell (p-1)^2 \mathcal{F}^2 + \lambda \ell (p^2 + 6p + 1)}{[2p\lambda \ell + (p-1)^2 \mathcal{F}]^2}, \quad (62)$$

where $\mathcal{F} = \tanh\left(\frac{\lambda \ell}{2}\right)$. In addition, we can also calculate the average energy density stored in the matrix, and we get

$$\frac{w_m}{E_b} = \frac{1}{2} e^{-2\lambda \ell} \frac{\lambda p(1+p)(1-p)^2}{2} \frac{2\mathcal{F} + \lambda \ell \mathcal{F}^2 - \lambda \ell}{[2p\lambda \ell + (p-1)^2 \mathcal{F}]^2}. \quad (63)$$

It is possible to prove that Eqs. (62) and (63) are in perfect agreement with Theorems 2 and 3, respectively. Importantly, we can easily verify, by directly adding the two energetic contributions, that $w_f + w_m = \frac{1}{2} \varepsilon^2 E_{eff,\infty}$, a result representing the energy balance stated for the general case in Theorem 4. We remark that if we let $E_t = E_b = E_f$ (i.e. $p=1$) in Eqs. (62) and (63) (Voigt model), we obtain $w_f = E_f \varepsilon^2$ and $w_m = 0$. Indeed, if the fibers have the same Young's modulus the energy contribution within the matrix must vanish and the total energy is adsorbed by the fibers ($\frac{1}{2} E_f \varepsilon^2$ for each fiber).

The knowledge of closed form expressions for the effective Young's modulus, Eq. (60), and the energetic contributions, Eqs. (62) and (63), allows us to introduce the concept of optimization of a bundle structure. The idea is that of maximizing the effective Young's modulus while minimizing the fiber energy density, which corresponds to attenuate the fiber mechanical solicitations

(compromise between stiffness and toughness). This optimal behavior can be obtained by introducing the efficiency function

$$\mathcal{E} = \frac{\varepsilon^2 E_{eff,\infty}}{2w_f} = 1 + \frac{w_m}{w_f} = 1 + \frac{(p-1)^2 (2\mathcal{F} + \lambda \ell \mathcal{F}^2 - \lambda \ell)}{2(p-1)^2 \mathcal{F} - \lambda \ell (p-1)^2 \mathcal{F}^2 + \lambda \ell (p^2 + 6p + 1)}, \quad (64)$$

to be maximized. The first line in Eq. (64) (proved through Theorem 4) means that the optimization of \mathcal{E} corresponds to maximize the fraction of energy adsorbed within the matrix or, conversely, to minimize the fraction of energy adsorbed within the fibers.

To show a specific example, we consider \mathcal{E} as function of $\sqrt{\kappa} \ell$, by maintaining fixed E_b and p (the elasticity of fibers). Importantly, we show in Fig. 5 that \mathcal{E} always exhibits a maximum, which corresponds to the characteristic length scale of the structure emerging from the optimization of the shear mechanism. Only when the contrast p approaches infinity, the curve \mathcal{E} versus $\sqrt{\kappa} \ell$ becomes monotonically increasing, without exhibiting any extremum point. This can be seen by performing the limit for $p \rightarrow \infty$ of Eq. (64), which gives the following result

$$\mathcal{E}(p \rightarrow \infty) = \frac{2}{1 + \frac{\sqrt{\kappa} \ell}{2\sqrt{E_b}} \left[\frac{1}{\tanh\left(\frac{\sqrt{\kappa} \ell}{2\sqrt{E_b}}\right)} - \tanh\left(\frac{\sqrt{\kappa} \ell}{2\sqrt{E_b}}\right) \right]}. \quad (65)$$

This asymptotic behavior is represented by the blue curves in Fig. 5. It is interesting to observe that for large values of the contrast p and large values of the length ℓ , the limit $\mathcal{E} = 2$ is approached, meaning that $w_m = w_f$, i.e. the total energy is equally distributed between matrix and fibers. This is the theoretical limit of the process, which transfers the adsorbed energy from the fibers to the matrix, thanks to the shear effects. We remark that the definition of \mathcal{E} , combined with Eq. (50), allows to write the two energy contributions in terms of \mathcal{E} and $w = w_f + w_m$, by eventually obtaining $w_f = \frac{1}{\mathcal{E}} w$ and $w_m = \left(1 - \frac{1}{\mathcal{E}}\right) w$. These expressions show how \mathcal{E} controls the distribution of energy between matrix and fibers.

The existence of optimal length scales for this simple structure suggests to use the same approach also for more complex heterogeneous bundles, which would more closely represent biological structures or composite nanomaterials.

5. Homogenization and optimization of complex structures

In this Section we exploit the general theory presented in Sections 2 and 3, in order to extend the optimization procedure to structures with more general heterogeneity. In particular, we study here the periodic staggered geometry (similar to a brick-and-mortar structure) and the staircase geometry (similar to a multi-step structure). These systems can represent both natural biological and artificial bioinspired structures. The bundle optimization is performed by considering the following efficiency function

$$\mathcal{E} = \frac{\varepsilon^2 E_{eff}}{2w_f} = 1 + \frac{w_m}{w_f} = 1 + \frac{\vec{v}^T \Omega^T \mathcal{R}^{-1} \mathcal{M} \Omega \vec{v}}{\vec{v}^T \Omega^T \mathcal{R}^{-1} \mathcal{J} \Omega \vec{v}} = 1 + \frac{\vec{v}^T \Omega^T \mathcal{W}^T \mathcal{M} \Omega \vec{v}}{\vec{v}^T \Omega^T \mathcal{W}^T \mathcal{J} \Omega \vec{v}}, \quad (66)$$

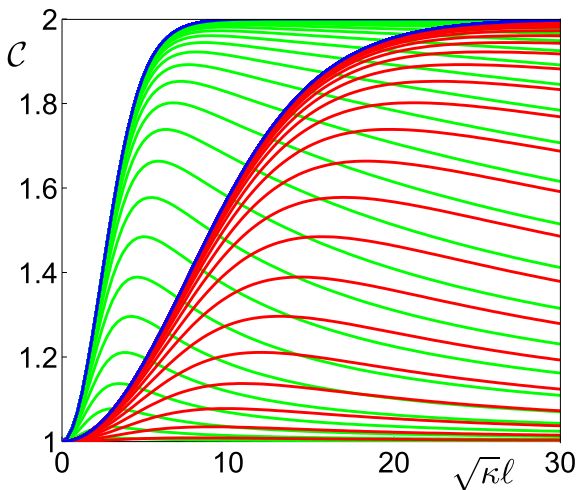


Fig. 5. Plot of the efficiency function \mathcal{E} , Eq. (64), versus $\sqrt{\kappa} \ell$. Two families of curves correspond to $E_b=1$ (green) and $E_b=10$ (red) and they are parametrized by $p=1.5^r$ with $r=1, \dots, 25$. The blue lines concern the case with $p \rightarrow \infty$, Eq. (65). (For interpretation of the references to colour in this figure legend, the reader is referred to the web version of this article.)

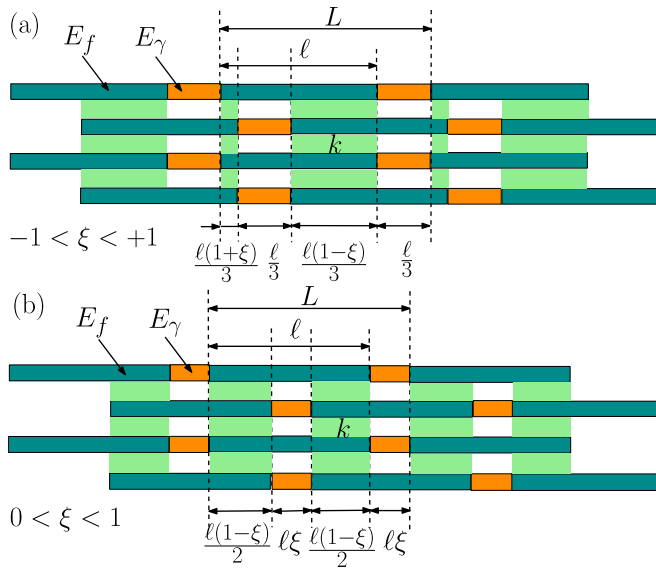


Fig. 6. Staggered periodic geometries: (a) asymmetric structure with sections lengths $(l_1, l_2, l_3, l_4) = (\ell/3(1+\xi), \ell/3, \ell/3(1-\xi), \ell/3)$, where $-1 < \xi < 1$; (b) symmetric structure with varying overlapping having sections lengths $(l_1, l_2, l_3, l_4) = (\ell/2(1-\xi), \ell\xi, \ell/2(1-\xi), \ell\xi)$, where $0 < \xi < 1$. In both schemes, E_f and E_γ represent the fibers and gaps Young's moduli, respectively and k is the interaction coefficient. Dark green segments represent the fibers, orange segments the gap regions, and light green areas the matrix connecting the overlapped fibers. (For interpretation of the references to colour in this figure legend, the reader is referred to the web version of this article.)

taking into account the energetic competition between fibers and matrix. The main idea is that of finding the most suitable geometry that is capable of transferring the largest amount of energy from the fibers to the matrix, thereby enhancing the shear efficiency.

5.1. Staggered geometry

We analyse here in detail the mechanical behavior of a staggered structure, similar to a brick wall. In particular, we take into consideration two specific geometries, as shown in Fig. 6. While in the first one we study the asymmetry effects, in the second one we consider the overlapping effects.

All staggered geometries can be represented with a periodic fiber bundle having a periodicity cell composed of four sections. In the first case, shown in Fig. 6(a), we can parametrize the sections lengths as $(l_1, l_2, l_3, l_4) = (\ell/3(1+\xi), \ell/3, \ell/3(1-\xi), \ell/3)$ (with $-1 < \xi < 1$), where ℓ represents the real length of the fiber (Young's modulus E_f) and ξ represents the asymmetry coefficient. Indeed, when $\xi \rightarrow -1$, the fibers overlapping is completely shifted on the right and, when $\xi \rightarrow +1$, the fibers overlapping is shifted on the left. In this structure, the gap between the fibers is fixed to the length $\ell/3$ (Young's modulus E_γ). In the second case, shown in Fig. 6(b), in order to analyse the overlapping effects we parametrize the sections lengths as $(l_1, l_2, l_3, l_4) = (\ell/2(1-\xi), \ell\xi, \ell/2(1-\xi), \ell\xi)$ (with $0 < \xi < 1$), where ℓ represents the fiber length as before, and ξ modulates the ratio between overlapping ($\ell/2(1-\xi)$) and gap ($\ell\xi$).

In Figs. 7 and 8 one can find the results for both geometries. In the first case, as expected, we obtain an effective Young's modulus E_{eff} and an efficiency function \mathcal{E} , which are symmetric with respect to ξ . Indeed, the configurations with the same shift on the left or on the right are completely equivalent from the mechanical point of view. The asymmetry, however, strongly influences the overall response. As regards the effective Young's modulus, we observe

that E_{eff} becomes vanishingly small for $\xi \rightarrow \pm 1$. In these cases, the overlapping among the fibers (i.e., the shear interactions) disappears on the left end-terminal of the periodicity cell ($\xi = -1$) or on the right end-terminal ($\xi = +1$), generating a very weak bundle section ($E_\gamma \ll E_f$), strongly degrading the effective stiffness. On the other hand, for $\xi = 0$, the overlapping regions are maximized, hence increasing the overall Young's modulus E_{eff} . The analysis of the efficiency function \mathcal{E} reveals that once fixed ξ , one can always find an optimal fiber length ℓ , maximizing \mathcal{E} . Moreover, we also remark that for ξ near ± 1 we need longer fibers in order to compensate the small overlapping region (on the left if $\xi \rightarrow -1$ or on the right if $\xi \rightarrow +1$). For the symmetrical structure with $\xi = 0$ we have the shortest optimal length since both overlapping regions are maximized. Finally, it is interesting to note that all optimal fiber lengths, corresponding to different values of ξ , yield the same value of the efficiency function \mathcal{E} . This point can be interpreted by observing that varying ξ we always have a constant total overlapping ($2\ell/3$) and, therefore, by choosing the proper fiber length, we can obtain the same overall bundle performances.

The behavior of the symmetric structure in Fig. 6(b) with varying overlapping is different and it can be found in Fig. 8. As for the effective Young's modulus, if $\xi \rightarrow 0$, then we have that $E_{eff} \rightarrow ME_f$, independently of ℓ , and it is the maximum stiffness we can achieve. Indeed, in this case the gaps disappear and we have, in the limit, a bundle of homogeneous fibers. Conversely, if $\xi \rightarrow 1$, then the overlapping regions of the fibers vanish and the overall Young's modulus becomes negligible ($E_\gamma \ll E_f$). The important point is that, for any value of ξ , we can always identify an optimal fiber length maximizing the efficiency function \mathcal{E} . Interestingly enough, the optimal fiber length is an increasing function of ξ . This can be simply explained by observing that for high values of ξ (with $0 < \xi < 1$) we reduce the overlapping regions and this loss of stiffness must be compensated by a longer system. We further observe that, contrarily to the previous case (see Fig. 7), the value of the efficiency function is not the same for all optimal fiber length. In fact, for different values of ξ , we have different sizes of the total overlapping region and this directly influences the effective performances of the bundle.

We also performed an analysis concerning the number M of fibers within the bundle. In particular, we considered a staggered structure with sections lengths $(l_1, l_2, l_3, l_4) = (\ell/3, \ell/3, \ell/3, \ell/3)$. It can be obtained by considering, e.g., the geometry in Fig. 7(a) with $\xi = 0$, or the geometry in Fig. 7(b) with $\xi = 1/3$. In Fig. 9 we show both the effective stiffness with the energetic contributions and the efficiency function to maximize. The effective Young's modulus and the energetic contributions are presented in panel (a). The same parameters are shown in panel (b) normalized by M ; we observe a very fast convergence of $E_{eff}M$, $2w_f/(\epsilon^2 M)$ and $2w_m/(\epsilon^2 M)$ for large values of M , as expected. In panel (c), we finally observe the effects of the number M of fibers on the efficiency function \mathcal{E} . We remark a slight reduction of the optimal fiber length ℓ in correspondence to values of M from 2 to ∞ . Moreover, as for the normalized effective Young's modulus, we have a fast convergence of the efficiency function to its limiting value.

To conclude the analysis of the staggered structure we also show some results concerning the effects of the gap Young's modulus on the efficiency function of the system. As before we considered the structure with $(l_1, l_2, l_3, l_4) = (\ell/3, \ell/3, \ell/3, \ell/3)$ and we plotted \mathcal{E} versus ℓ in Fig. 10. We note a sensible variation of the optimal length in terms of E_γ and, for vanishingly small values of E_γ , we observe a convergence of the optimal fiber length to a specific finite value.

5.2. Staircase geometry

This Section deals with the periodic staircase geometry,

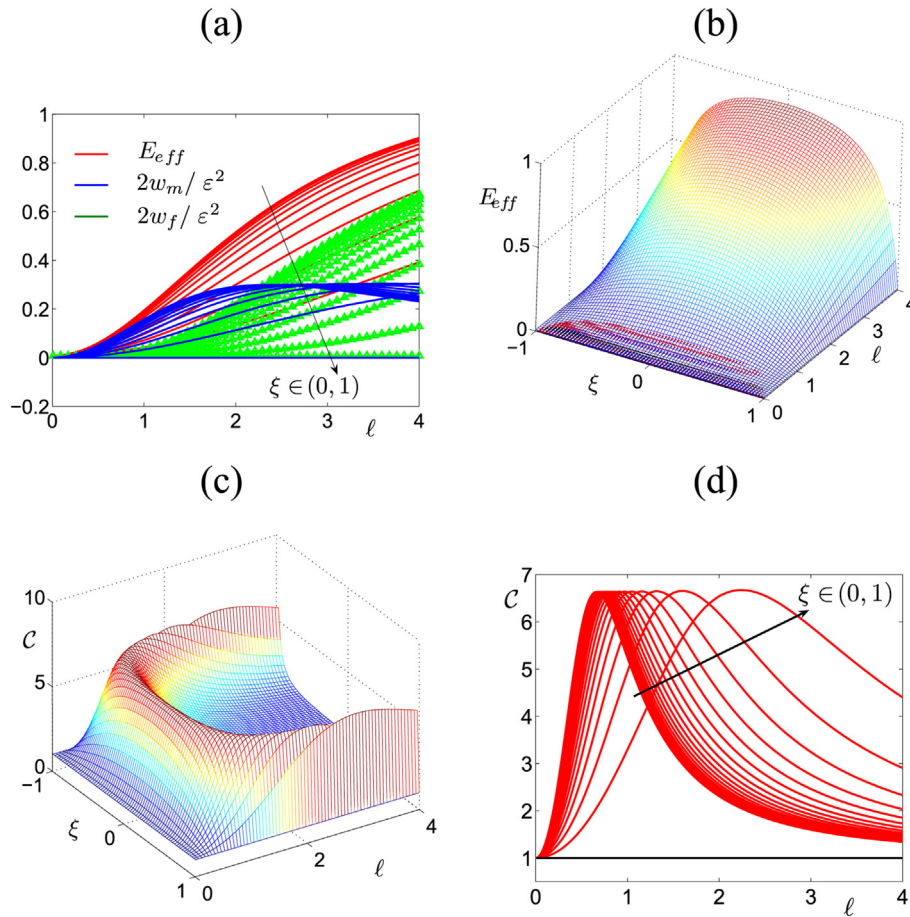


Fig. 7. Homogenization and optimization of the asymmetric staggered structure shown in Fig. 6(a). The lengths of the sections are $(l_1, l_2, l_3, l_4) = (\ell/3(1 + \xi), \ell/3, \ell/3(1 - \xi), \ell/3)$ with $-1 < \xi < 1$. The effective Young's modulus and the energy contributions are represented in panel (a) versus ℓ and parametrized by the asymmetry coefficient ξ . In panels (b) and (c) E_{eff} and ℓ are shown versus ξ and ℓ . The symmetry with respect to $\xi=0$ can be observed in both surfaces. Finally, \mathcal{C} versus ℓ is represented in panel (d) for 25 equispaced values of ξ in $(0,1)$. We used the parameters $E_f=1, E_\gamma=1/1000, k=1$ and $M=2$ (in a.u.).

represented in Fig. 11. This configuration can be described as follows. The spatial period is given by $L=\ell+\gamma$ where ℓ is the fiber length and γ is the gap extension. Starting from the first (bottom) fiber, the second one is left-shifted by a displacement $\ell-\delta$. Thus, δ represents the overlapping between two adjacent fibers, as shown in Fig. 11 (light green areas). We repeat this procedure n times and we obtain the last fiber in the same translational position of the first one. The resulting structure is shown in Fig. 11 for $n = 2, 3, 4$ and 5. The red frames in this scheme represent the periodic cells in both the longitudinal and transverse directions. Of course, to generate this structure, the parameters ℓ, δ and γ can not be independent and must fulfill the following constraints. By construction, $\ell+\gamma=n(\ell-\delta)$, which means that $\frac{\ell+\gamma}{\ell-\delta}$ must be an integer number. Further, from the relation $n = \frac{\ell+\gamma}{\ell-\delta}$, once l and δ are fixed, we have $\gamma = (n - 1)\ell - n\delta$. We assume that, both on the left and on the right of the gap segment (of length γ), we always have two regions with a given finite overlapping between adjacent fibers. It implies that $\delta>0, \gamma>0$ and $\ell-\delta-\gamma>0$. From $\gamma>0$ we can prove that $\frac{\delta}{\ell} < \frac{n-1}{n}$. Similarly, from $\ell-\delta-\gamma>0$ we obtain that $\frac{\delta}{\ell} > \frac{n-2}{n-1}$. Therefore, for the ratio δ/ℓ , the admissibility interval is $\frac{n-2}{n-1} < \frac{\delta}{\ell} < \frac{n-1}{n}$. To conclude the structure definition, we also assume that the total number of fibers is given by $M=nB$, where n determines the order of the staircase geometry and B represents the number of blocks (red frames in Fig. 11) considered within the bundle.

The properties of the staircase bundle geometry are reported in Fig. 12, where we show the effective Young's modulus and the efficiency function for $n = 2, 3, 4$ and 5. We represented the results for all orders n in the same plot since the admissibility intervals for δ/ℓ do not overlap for different n , and cover the whole interval $(0,1)$ for $n=1, \dots, +\infty$.

The two limiting cases can be analysed by considering $\frac{\delta}{\ell} \rightarrow \frac{n-1}{n}$ or $\frac{\delta}{\ell} \rightarrow \frac{n-2}{n-1}$. In the first case we have the overlap $\ell-\delta-\gamma$ approaching zero and, therefore, a vanishingly small effective stiffness (since $E_\gamma \ll E_f$). In the second case the gap extension γ approaches zero, hence $E_{eff}=ME_f=nBE_f$ (i.e., a bundle of homogeneous fibers). This behavior can be seen in Fig. 12(a). In both limiting cases the efficiency function \mathcal{C} is negligibly small since the energy accumulated in the matrix is very small in such conditions. However, one can always find an optimal fiber length ℓ for any value of the ratio δ/ℓ , as one can easily deduce from Fig. 12(b).

Fig. 13 displays both the effective stiffness with the corresponding energetic contributions and the efficiency function to maximize for $n = 2, \dots, 8$. We considered a staircase structure with $\frac{\delta}{\ell} = \frac{2n^2-4n+1}{2n(n-1)}$. This value corresponds to the mean value of the endpoints of the admissibility interval $(\frac{n-2}{n-1}, \frac{n-1}{n})$. Moreover, we take $\gamma = (n - 1)\ell - n\delta$, as before. In panel (b) of Fig. 13, we can observe the effects of the number n of fibers in a given block

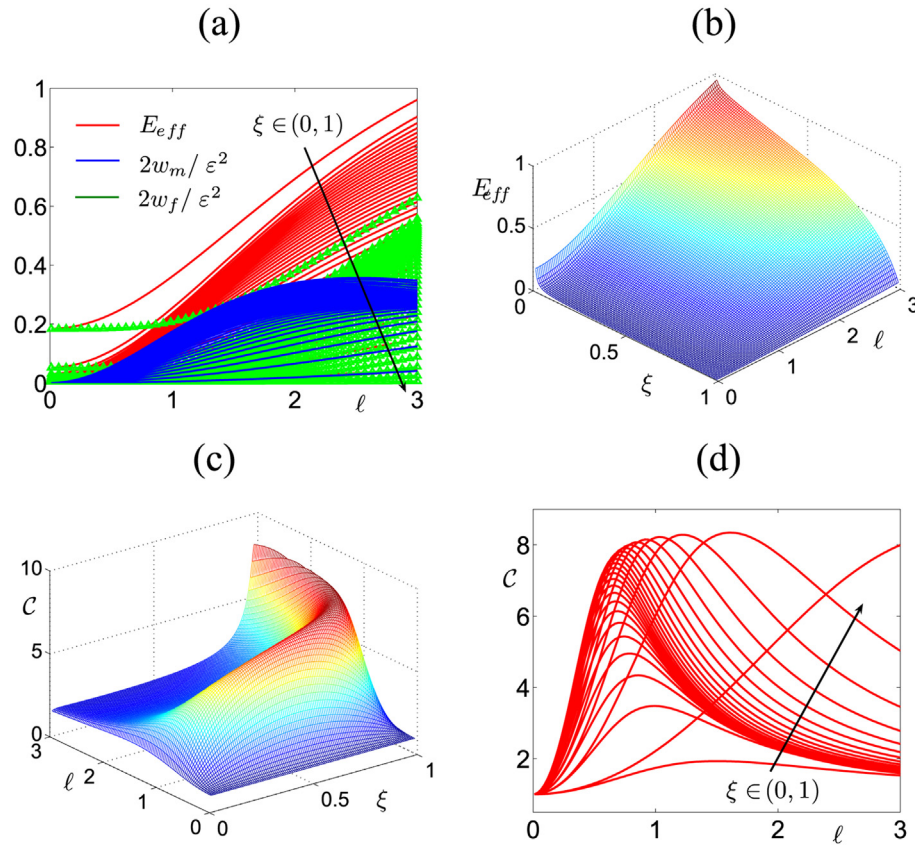


Fig. 8. Homogenization and optimization of the symmetric staggered structure with varying overlapping shown in Fig. 6(b). The lengths of the sections are $(l_1, l_2, l_3, l_4) = (\ell/2(1-\xi), \ell\xi, \ell/2(1-\xi), \ell\xi)$ with $0 < \xi < 1$. In panel (a) the effective Young's modulus is shown together with the energy contributions versus the fiber length ℓ (and parametrized by the overlapping coefficient ξ). A three-dimensional representation of E_{eff} and \mathcal{C} can be found in panels (b) and (c), respectively. Finally, \mathcal{C} versus ℓ is represented in panel (d) for 25 equispaced values of ξ in $(0,1)$. We used the parameters $E_f=1$, $E_\gamma=1/1000$, $k=1$ and $M=2$ (in a.u.).

($B=1$) on the efficiency function \mathcal{C} . We remark a sensible increase of the optimal fiber length ℓ in correspondence to values of n from 2 to 8.

A further analysis can be performed for the number B of blocks within the staircase bundle. As an example, we considered a specific structure with $n=3$, $\frac{\delta}{\ell} = \frac{2n^2-4n+1}{2n(n-1)} = \frac{7}{12}$ and $\frac{\gamma}{\ell} = (n-1) - n\frac{\delta}{\ell} = \frac{1}{4}$. In Fig. 14 we show both the normalized effective stiffness with the corresponding energetic contributions and the efficiency function to maximize. The effective Young's modulus and the energetic contributions are presented in panel (a), normalized by $M = nB$. As expected, all the quantities $E_{eff}/(nB)$, $2w_f/(\epsilon^2 nB)$ and $2w_m/(\epsilon^2 nB)$ converge rapidly for large values of B . In panel (b), the effects of the total number of fibers on the efficiency function \mathcal{C} are shown. We remark a rather slight reduction of the optimal fiber length ℓ in correspondence to values of B from 1 to 8. Moreover, as for the normalized effective Young's modulus, we have a fast convergence of \mathcal{C} to its limiting value.

To conclude the analysis of the periodic staircase structure we also show some results concerning the effects of the gap Young's modulus on the efficiency function of the system. As before we considered the structure with $n=3$, $\delta/\ell=7/12$ and $\gamma/\ell=1/4$ and we plotted \mathcal{C} versus ℓ in Fig. 15. We note a sensible variation of the optimal length in terms of E_γ and, for vanishingly small values of E_γ , we observe a convergence of the optimal fiber length to a specific finite value.

6. Comparison with real biological structures

In this Section, the optimization procedure based on Eq. (66) is directly applied to four biological systems: sarcomere, collagen, abalone nacre and spider silk. For these structures we evaluate both the characteristic length scales of the periodic cell, and the overlap regions among fibers. The theoretical results are then compared with available experimental data. We remark that the interaction among fibers sensibly depends on their cross-sectional geometry. In particular, in natural systems we can mostly find cylindrical or parallelepipedal fibers. As a matter of fact, while the unit cell of sarcomere and collagen can be simplified by considering actin, myosin and titin (for sarcomere), and tropocollagen triple helix (for collagen) as cylindrical filaments, the architecture of nacre shells and spider silks presents parallelepipedal fibers (aragonite platelets in the first case and beta-sheets in the second one). Of course, these geometrical simplifications do not take into account the real complexity of biological systems. For instance, the consideration of a single interaction coefficient k smears out the refined effects of the hydrogen bonds and the Van der Waals interactions between the macromolecules of the bundle. However, this approximation is typically adopted to study bundles of biological origin and several results based on this assumption have been successfully compared with numerical simulations and experiments (Buehler, 2006, 2008; Chen et al., 2009; Wei et al., 2012). The dependence of the interaction coefficient k on the shape of fibers and the shear modulus μ of the matrix can be studied as follows. Since the sliding among

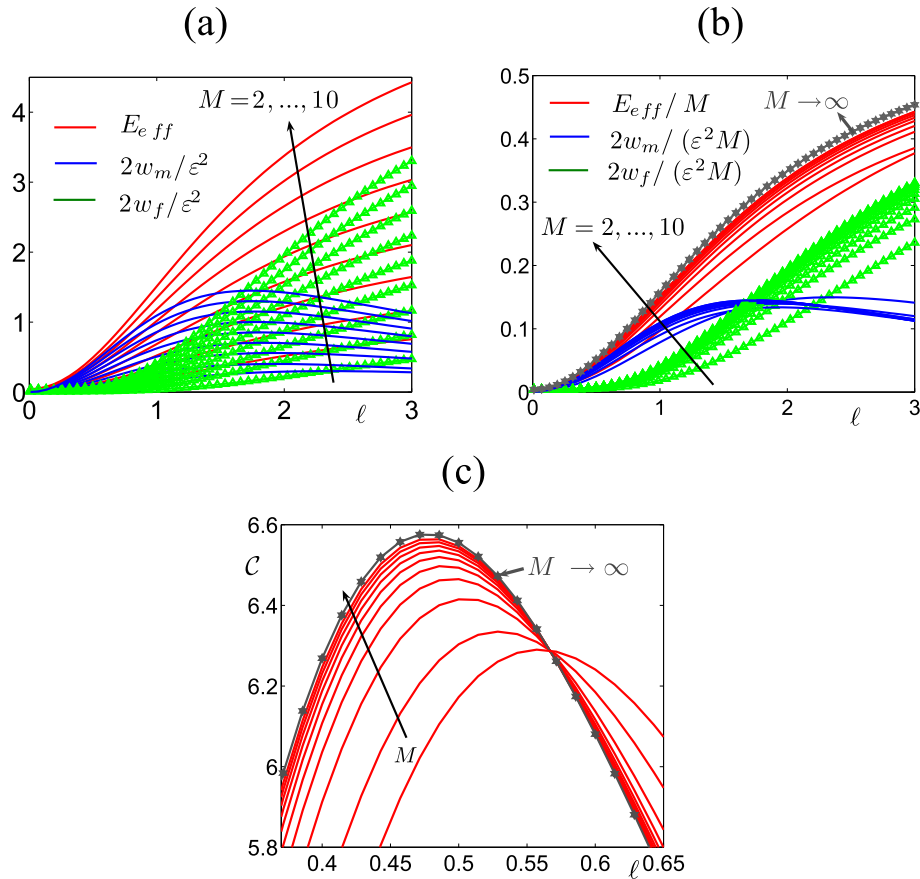


Fig. 9. Analysis of the staggered structure $(l_1, l_2, l_3, l_4) = (\ell/3, \ell/3, \ell/3, \ell/3)$ versus the number M of fibers. Panel (a): effective modulus and energetic contributions as function of ℓ for $M=2, \dots, 10$. Panel (b): the same quantities are divided by M . These normalized values show a fast convergence for $M \rightarrow \infty$. Panel (c): zoom of \mathcal{C} versus ℓ for $M \in \{3, 2n; n = 2, \dots, 10\}$. Also in this case, a fast convergence can be observed with a slight modification of the optimal fiber length. We used the parameters $E_f=1$, $E_\gamma=1/1000$ and $k=1$ (in a.u.).

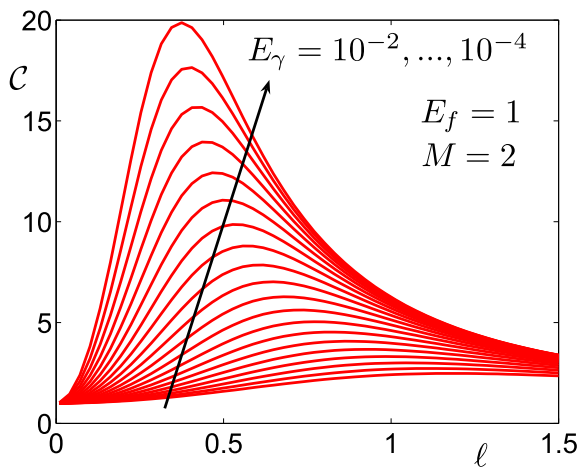


Fig. 10. Analysis of the effects of the gap Young's modulus E_γ on the efficiency function \mathcal{C} of the staggered structure defined by $(l_1, l_2, l_3, l_4) = (\ell/3, \ell/3, \ell/3, \ell/3)$ (we used $k=1$ in a.u.). The function \mathcal{C} is plotted versus ℓ for 20 equispaced values of E_γ in the range 10^{-2} – 10^{-4} .

fibers represents an anti-plane shear elastic problem, we can easily exploit the analogy with electrostatics to obtain $k=k(\mu)$ for two adjacent fibers. The interaction coefficient for a pair of infinite-length parallel cylindrical fibers can be eventually obtained as (Cox, 1952)

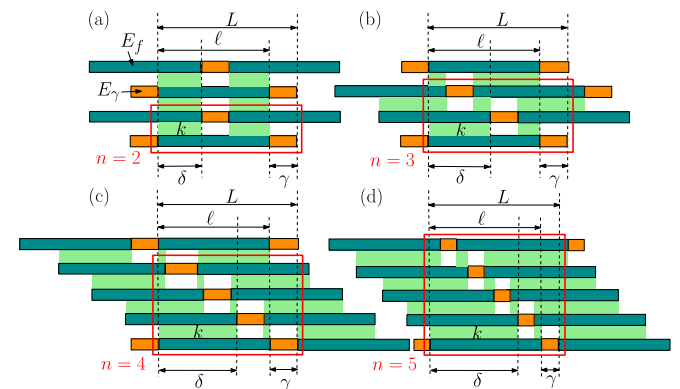


Fig. 11. Staircase geometry with $\ell > 0$, $\delta > 0$, $\gamma > 0$ and $\ell - \delta - \gamma > 0$. The periodic structures are defined by the relations $n = \frac{\ell + \gamma}{\delta}$ and $\gamma = (n-1)\ell - n\delta$. Then, the condition $\frac{n-2}{n-1} < \frac{\delta}{\ell} < \frac{n-1}{n}$ must be always verified. In panel (a), (b), (c) and (d) the geometries for $n = 2, 3, 4$ and 5 are shown. The quantities E_f , E_γ and k represent the fiber Young's modulus, the gap Young's modulus and the interaction coefficient.

$$k = \frac{\mu}{r^2 \ln \left(\frac{d}{2r} + \sqrt{\frac{d^2}{4r^2} - 1} \right)} \approx \frac{\mu}{r^2 \ln \frac{d}{r}}, \quad (67)$$

where r is the fibers radius and d is the distance between the centres. The approximation in Eq. (67) is valid for $d \gg r$. On the

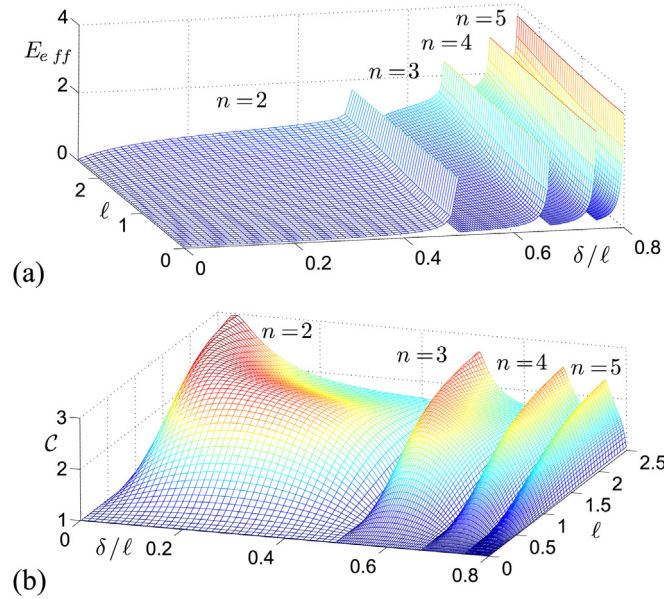


Fig. 12. Effective Young's modulus E_{eff} [panel (a)] and efficiency function \mathcal{C} [panel (b)] for the periodic staircase structures as function of ℓ and δ/ℓ with $n = 2, 3, 4$ and 5 (see Fig. 11). For each value of n , we have $\frac{n-2}{n-1} < \frac{\delta}{\ell} < \frac{n-1}{n}$ (non-overlapping intervals). We observe an optimal fiber length ℓ for any admissible value of δ/ℓ . We used the parameters $E_f=1$, $E_\gamma=1/100$, $k=1$ and $B=1$ (in a.u.).

other hand, the interaction coefficient for two infinite-length parallel parallelepipedal fibers is given by (Wei et al., 2012)

$$k = \frac{\mu}{rd}, \tag{68}$$

where r is the fiber thickness and d is the distance between two adjacent sides. Note that, since these relations are obtained for a couple of fibers, they become approximated when used for a system of fibers with $M > 2$. In the following calculations we accept this approximation and we maintain k constant independently of the number of fibers.

6.1. Sarcomere

Firstly, we apply the proposed technique to find the optimal overlap length scale of contiguous actin and myosin-titin fibers in a sarcomere of muscle tissue. The sarcomere is composed of thin actin filaments (with a radius $r_A \sim 3.5$ nm) and thick myosin filaments ($r_M \sim 7.5$ nm) connected with titins ($r_T \sim 0.5$ nm) (Geoffrey, 2000), as shown in Fig. 16(a). The sarcomere length ranges from 1.32 to 3.20 μ m (Thomas and Richard, 2001; Hamrell and Hultgren, 1992; Dimery, 1985; Weijss et al., 1983). Chemical and physical interactions between actin and myosin filaments cause the sarcomere length to change (sliding filament theory). This is possible because of a variable overlapping between actin and myosin-titin fibers (Kawai and Brandt, 1980; Ford et al., 1981). However, we

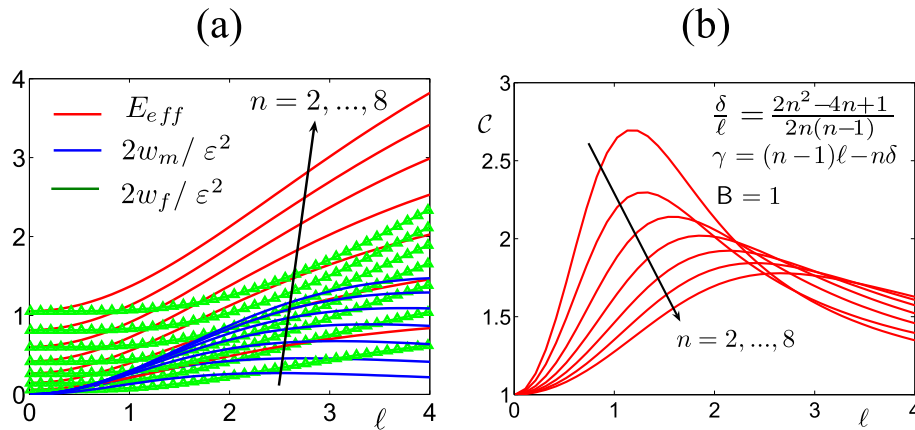


Fig. 13. Analysis of the effects of n on the periodic staircase structure. Panel (a): effective Young's modulus and energetic contributions. Panel (b): \mathcal{C} versus ℓ for $n = 2, \dots, 8$. For any value of ℓ we fixed $\frac{\delta}{\ell} = \frac{2n^2 - 4n + 1}{2n(n-1)}$, representing the mean value of the endpoints of the admissibility interval $(\frac{n-2}{n-1}, \frac{n-1}{n})$, and $\gamma = (n-1)\ell - n\delta$. We used the parameters $E_f=1$, $E_\gamma=1/100$, $k=1$ and $B=1$ (in a.u.).

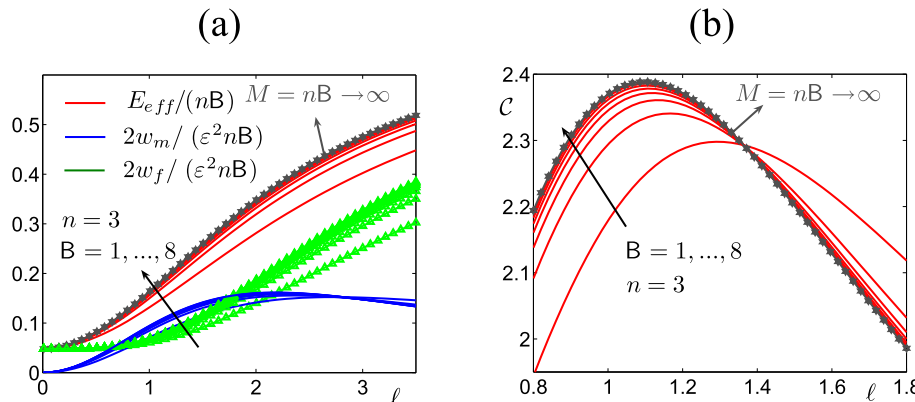


Fig. 14. Analysis of the effects of B on the periodic staircase structure (for $n=3$). We imposed $\delta/\ell=7/12$ (mean value of the endpoints of the admissibility interval) and $\gamma/\ell=1/4$. Panel (a): normalized values $E_{eff}/(nB)$, $2w_f/(\epsilon^2 nB)$ and $2w_m/(\epsilon^2 nB)$ versus the fiber length ℓ . Panel (b): \mathcal{C} versus ℓ for $B=1, \dots, 8$. Both $E_{eff}/(nB)$ and \mathcal{C} show a convergent behavior for $M=nB \rightarrow \infty$. We used the parameters $E_f=1$, $E_\gamma=1/100$ and $k=1$ (in a.u.).

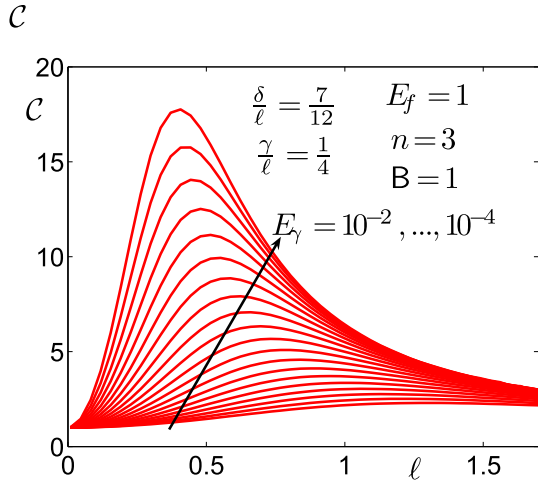


Fig. 15. Analysis of the effects of the gaps Young's modulus on the periodic staircase structure with $n=3$ and $B=1$. Since $n=3$, we imposed $\delta/l=7/12$ (mean value of the endpoints of the admissibility interval) and $\gamma/l=1/4$. For vanishingly small values of E_γ , we observe a convergence of the optimal fiber length to a finite value.

underline that here we consider the passive response of the sarcomere, i.e., its elasticity measured without active phenomena. The myosin and titin Young's moduli have been experimentally determined as $E_f^M \sim 10$ GPa (Kojima et al., 1994) and $E_f^T \sim 0.7$ GPa (Abolbashi and Ameli, 2012), respectively. Experiments also probed the Young's modulus of a single actin filament to be $E_f^A \sim 1.8$ GPa (Kojima et al., 1994). Their interaction is supposed here to be controlled by the shear modulus of F-actin gel, which has been estimated to be $\mu \sim 10$ kPa (Satcher and Forbes, 1996; Jacot et al., 2010). For obtaining the optimal overlap length δ between actin and myosin-titin filaments, we substituted these parameters in our model, considering $M = 10$ fibers (the results remain substantially unaltered if $M \gg 10$, as shown in Fig. 9). In this case, δ represents the overlap region among filaments, while γ is the length of the region where filaments do not interact (see Fig. 16(a)). The periodic cell is represented in Fig. 16(c). In this case, fibers have four different Young's moduli, $E_f^A, E_f^M, E_f^T, E_\gamma$, representing the elastic moduli of actin, myosin, titin, and H-zone (gap), respectively. The first three elastic moduli have been fixed equal to the experimental values previously reported, while the elastic moduli of the H-zone has been fixed to $E_\gamma = 10$ Pa, for representing an ideally empty region. The interaction among filaments is represented by an

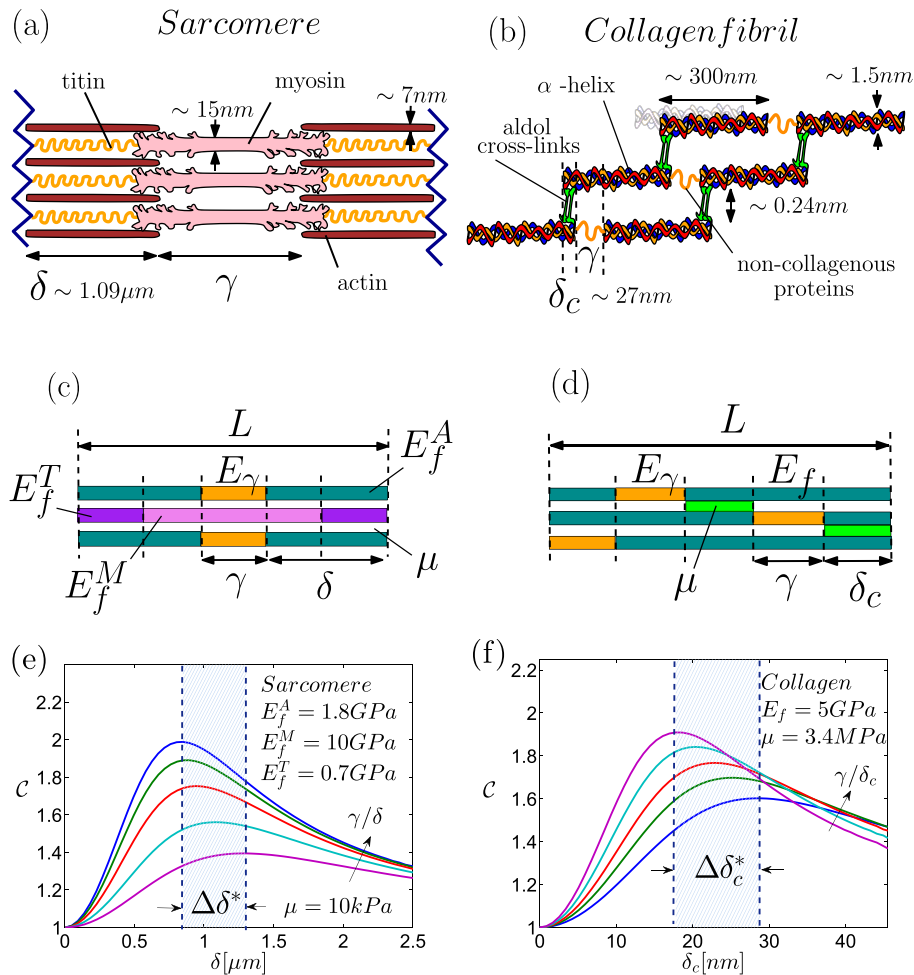


Fig. 16. Panel (a) and (b): representation of the sarcomere and collagen fibril structures. Panel (c) and (d): schematics of the periodic cell adopted in the analysis. Panel (e) and (f): efficiency function \mathcal{C} exhibiting the maximum point in correspondence to the specific overlapping length scales δ^* (or δ_c^*). The ratio γ/δ (or γ/δ_c) varies in the range specified in Table 1. Shaded areas represent the range of variation of the optimal overlapping lengths.

Table 1
Physical and geometrical parameters adopted for modeling the biological architectures and obtained optimal length scales.

Structure	E_f (GPa)	E_γ (GPa)	μ (GPa)	γ/δ (or γ/δ_c)	δ^* (or δ_c^*) (μm)	L^* (μm)
Sarcomere	0.7–10	1×10^{-8}	10^{-5}	0.003–0.13	0.85–1.30	1.70–2.77
Collagen	5	1	3.4×10^{-3}	1–2	$17.8\text{--}28.8 \times 10^{-3}$	$318\text{--}334 \times 10^{-3}$
Nacre	106	1×10^{-6}	1.4	$0.3\text{--}1 \times 10^{-7}$	0.656–1.72	1.31–3.44
Spider Silk	22.6	5×10^{-2}	4.6	$0.9\text{--}1 \times 10^{-3}$	$1.15\text{--}2.2 \times 10^{-3}$	$2.3\text{--}4.4 \times 10^{-3}$

elastic matrix with the shear modulus μ of F-actin gel. Moreover, we remark that Eq. (67) is valid only for two parallel cylindrical fibers with identical radius r . Consequently, we considered fibers having the same average radius: for actin and myosin r was set equal to $(r_A + r_M)/2 = 5.5 \mu\text{m}$. With these values, we obtain an optimal overlap length δ^* ranging from 0.85 to $1.30 \mu\text{m}$. Fig. 16 (e) reports these results, showing the range of variation of δ^* for five equispaced values of the ratio γ/δ in the interval (0.003, 0.13) (this range being deduced from electron micrograph (Kossmann and Huxley, 1961)). These optimal overlaps correspond to a total sarcomere length $L^* = 2\delta^* + \gamma = 1.70\text{--}2.77 \mu\text{m}$. This is in very good agreement with experimental results (Thomas and Richard, 2001; Hamrell and Hultgren, 1992; Dimery, 1985; Weijs et al., 1983). All the parameters used in the model and the obtained lengths are summarized in Table 1.

6.2. Collagen

A second application of the model is consecrated to collagen-I fibrils, with the aim of finding the optimal overlap length scale of contiguous tropocollagen molecules. In particular, we consider non-mineralized collagen fibrils, which are typically composed of an organic phase of 90% type-I collagen and 10% non-collagenous proteins (NCP). Tropocollagen molecules have a triple α -helical structure made up of 3 different amino-acids (Ramachandran and Kartha, 1955) having a radius of $\sim 1.5 \text{ nm}$ (Orgel et al., 2001) and length $\ell \sim 300 \text{ nm}$ (Gautieri et al., 2011), as shown in Fig. 16(b). This staircase geometry exhibits a distance between two fibers of $\sim 0.24 \text{ nm}$ and molecules are organized in very long periodic assemblages called fibrils (Landis et al., 1993). The structure is supported by the aldol cross-links between molecules. The D-periodic gap/overlap spacing is characterized by an overlap length $\delta_c \sim 27 \text{ nm}$ and by a

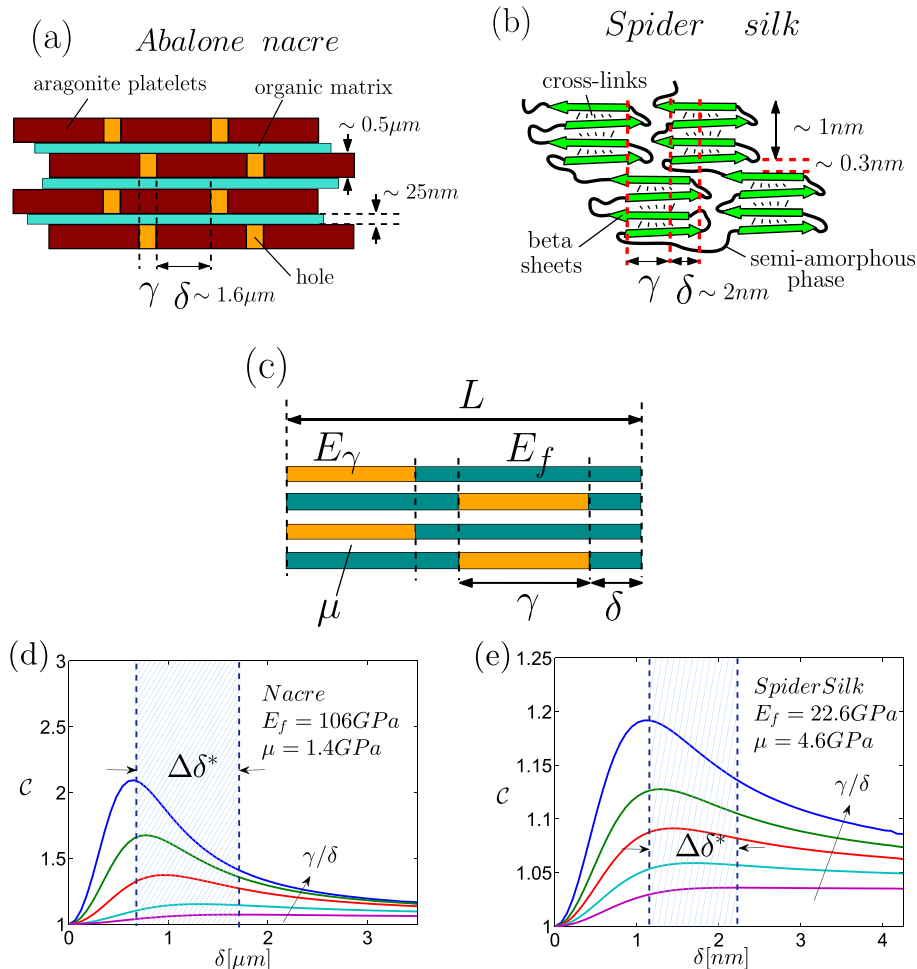


Fig. 17. Panel (a) and (b): representation of the abalone nacre and spider silk structures. Panel (c): schematic of the periodic cell adopted in the analysis of both systems. Panel (d) and (e): efficiency function c exhibiting the maximum point in correspondence to the specific overlapping length scales δ^* . The ratio γ/δ varies in the range specified in Table 1. Shaded areas represent the range of variation of the optimal overlapping lengths.

gap length $\gamma \sim 40$ nm (Hodge and Schmitt, 1960). In terms of the geometry defined in Section 5.2, we have that $\delta = \ell - \delta_c - \gamma \approx 233$ nm and, therefore, the order of the periodic staircase collagen structure is $n = \frac{\ell + \gamma}{\ell - \delta} = 5$. Stretching experiments report the Young's modulus of a single collagen molecule in the range $E_f \sim 0.35 - 12$ GPa (Sun et al., 2002), while the non-collagenous proteins have an elastic modulus $E_\gamma \sim 1$ GPa (Nikolov and Raabe, 2008). The interaction among molecules measured via micromechanical experiments reported the shear modulus of aldol cross-links $\mu \sim 3.4$ MPa (Yang et al., 2008). Substituting these values in our model, and using the periodic cell represented in Fig. 16(d) with $M = 10$ fibers ($B = 2$), we obtain an optimal overlap length δ_c^* ranging from ~ 17.8 to ~ 28.8 nm, which is again in very good agreement with experimental findings by electron microscopic tomography (Landis et al., 1993). Fig. 16(f) reports these results, showing the range of variation of δ_c^* obtained with five different values of the ratio γ/δ_c^* in the interval (1,2). The optimal overlaps correspond to an optimal length of the unit-cell $L^* = 318 - 334$ nm (see Table 1 for details).

6.3. Abalone nacre

As a third case, we analyse the structure of the red abalone nacre to obtain the optimal overlap length among aragonite platelets, which leads to the best load sharing between fibers and matrix. In Fig. 17 (a) the microstructure of nacre is shown. The aragonite platelets (thickness $\sim 0.5 \mu\text{m}$) and the organic matrix (thickness ~ 25 nm) are assembled in the typical brick and mortar (staggered) geometry (Barthelat et al., 2006). The longitudinal distance between platelets is $\gamma \sim 25$ nm, as measured by transmission electron microscopy, scanning electron microscopy, and atomic force microscopy observations (Barthelat et al., 2006; Lin and Meyers, 2005). Stretching experiments reported the Young's modulus of a single aragonite platelet $E_f \sim 106$ GPa (Tang et al., 2007). Along the short edges, the aragonite platelets are not in contact with any organic matrix (Lin and Meyers, 2005; Tang et al., 2007), thus the Young's modulus in the gap region E_γ is negligible with respect to E_f (Bertoldi et al., 2008). The interaction among platelets is considered via the shear modulus of the organic matrix, which has been measured to be $\mu \sim 1.4$ GPa (Jackson et al., 1988). With these values, and the periodic cell represented in Fig. 17(c) with $M = 10$ fibers, we obtain an optimal overlap length δ^* ranging from ~ 0.656 to $\sim 1.72 \mu\text{m}$. This is in quite good agreement with microscopic characterizations that found an overlap length of the red abalone nacre to be of $\sim 1.6 \mu\text{m}$ (Espinosa et al., 2011). Fig. 17(d) reports these results for five different values of the ratio γ/δ in the interval $(0.3, 1) \times 10^{-7}$. The optimal overlaps correspond to an optimal length of the unit-cell $L^* = 1.31 - 3.44 \mu\text{m}$ (see Table 1 for details).

6.4. Spider silk

The last example concerns the optimal overlap length among beta-sheets in spider silk structures. In Fig. 17(b) the microstructure of the spider silk is shown. It is composed of crystalline blocks of alanine and glycine, arranged in parallel beta-sheets (thickness ~ 1 nm) and a matrix of amorphous-like helical structures (thickness ~ 0.3 nm), composed essentially by glycine. This platelet-matrix structure is held together by a network of hydrogen-bond cross-links (Van Beek et al., 2002). As for the abalone nacre, the geometry can be generally described with the brick and mortar staggered assemblage (Wei et al., 2012). The extremely small length scale of this structure makes experiments very difficult to be performed. Thus, the Young's modulus of a single beta sheet could be only estimated by means of large-scale molecular dynamics simulations

that predicted $E_f \sim 22.6$ GPa (Keten et al., 2010). Similarly, the interaction among beta-sheets is mediated by the shear modulus of cross-links, which assumes the calculated value $\mu \sim 4.6$ GPa (Keten et al., 2010). Along the edge extremities, beta-sheets are linked together with a semi-amorphous phase, for which the Young's modulus has been fixed to $E_\gamma \sim 50$ MPa. These values, considered in the same periodic cell used for nacre with $M = 10$ fibers, gave an optimal overlap length δ^* ranging from ~ 1.15 to ~ 2.2 nm and a corresponding unit-cell length of $2.3 - 4.4$ nm, which is in agreement with experimental observations in which the length of beta-sheets was measured in the range $2 - 8$ nm (Penel et al., 2003). Fig. 17(e) reports these results for five different values of the ratio γ/δ in the interval $(0.9, 1) \times 10^{-3}$ (see Table 1 for details).

7. Summary and conclusion

In this work, we developed a Floquet-based homogenization and optimization theory for the elastic behavior of periodic heterogeneous fiber bundles with arbitrary geometry. We considered longitudinal-periodic structures with a given number of heterogeneous fibers subject to arbitrary mutual interactions. This "shear-lag" arrangement can be found in several biological structures in which hard fibers are embedded in a soft matrix with a regular geometry. Our Floquet-based approach is able to analyse the overall stiffness and the energy distribution between fibers and matrix. In particular, we obtained closed-form expressions for the effective Young's modulus E_{eff} and the average energy densities in the fibers (w_f) and in the matrix (w_m), respectively. The knowledge of the relative energetic contributions of fibers and matrix is necessary to introduce an efficiency function \mathcal{E} , which must be maximized for obtaining optimal bundle structures. The underlying idea is that of transferring, as much as possible, the elastic energy stored in the system from the fibers (hard material subject to brittle fracture) to the matrix (soft material with high fracture toughness). In this respect, we defined the efficiency function as the ratio between the average energy accumulated in the fibers and the average energy within the matrix. We then showed that this function always exhibits a maximum in correspondence of a specific length scale, characterizing the geometry of the natural bundle structure. It is important to underline that our optimality criterion, based on energetic arguments, is coherent with the general criteria for the elastic or inelastic crack growth. Interestingly, the theory can be applied both to natural and artificial composite systems.

Finally, through our optimal criterion, we obtained the characteristic length scales of the periodic cell for a number of biostructures, such as nacre shells, muscle sarcomeres, collagen fibrils and spider silks. This length scale corresponds to the structure that allows to maximize the load transfer to the matrix, thereby minimizing the possibility of fracture within the fibers. For all the investigated structures, the recovered length scales are in very good agreement with available experimental data.

References

- Abolbashi, M.H., Ameli, S., 2012. Mechanical unfolding of titin I27 domain: nanoscale simulation of mechanical properties based on virial theorem via steered molecular dynamics technique. *Sci. Iran.* 19 (6), 15261533.
- Ashby, M.F., Gibson, L.J., Wegst, U., Olive, R., 1995. The mechanical properties of natural materials. I. Material property Charts. *Proc. R. Soc. Lond. A* 450, 123–140.
- Barthelat, F., Lia, C.H., Comia, C., Espinosa, H.D., 2006. Mechanical properties of nacre constituents and their impact on mechanical performance. *J. Mater. Res.* 21 (8), 1977–1986.
- Ben-Israel, A., Greville, T.N.E., 2003. *Generalized Inverses: Theory and Applications*. Springer-Verlag, New York.
- Bertoldi, K., Bigoni, D., Drugan, W.J., 2008. Nacre: an orthotropic and bimodular elastic material. *Compos. Sci. Technol.* 68, 13631375.

- Beyerlein, I.J., Phoenix, S.L., 1996. Stress concentrations around multiple fiber breaks in an elastic matrix with local yielding or debonding using quadratic influence superposition. *J. Mech. Phys. Solids* 44, 1997.
- Beyerlein, I.J., Phoenix, S.L., Raj, R., 1998. Time evolution of the stress redistribution around multiple fiber breaks in a composite with viscous and viscoelastic matrices. *Int. J. Solids Struct.* 35, 3177.
- Bosia, F., Abdalrahman, T., Pugno, N.M., 2012. Investigating the role of hierarchy on the strength of composite materials: evidence of a crucial synergy between hierarchy and material mixing. *Nanoscale* 4, 1200.
- Buehler, M.J., 2006. Nature designs tough collagen: explaining the nanostructure of collagen fibrils. *PNAS* 103, 12285–12290.
- Buehler, M.J., 2008. Molecular architecture of collagen fibrils: a critical length scale for tough fibrils. *Curr. Appl. Phys.* 8, 440–442.
- Chen, B., Wu, P.D., Gao, H., 2009. A characteristic length for stress transfer in the nanostructure of biological composites. *Compos. Sci. Technol.* 69, 1160–1164.
- Colombo, L., Giordano, S., 2011. Nonlinear elasticity in nanostructured materials. *Rep. Progr. Phys.* 74, 116501.
- Cox, H.L., 1952. The elasticity and strength of paper and other fibrous materials. *Br. J. Appl. Phys.* 3, 72–79.
- Cranford, S.W., 2013. Increasing silk fibre strength through heterogeneity of bundled fibrils. *J. R. Soc. Interface* 10, 20130148.
- Cranford, S.W., Tarakanova, A., Pugno, N.M., Buehler, M.J., 2012. Nonlinear material behaviour of spider silk yields robust webs. *Nature* 482, 72–76.
- Daniels, H.E., 1945. The statistical theory of the strength of bundles of threads. *Proc. R. Soc. Lond. Ser. A* 183, 405.
- Dimery, N.J., 1985. Muscle and sarcomere lengths in the hind limb of the rabbit (*Oryctolagus cuniculus*) during a galloping stride. *J. Zool.* 205, 373383.
- Espinosa, H.D., Juster, A.L., Latourte, F.J., Loh, O.Y., Gregoire, D., Zavattieri, P.D., 2011. Tablet-level origin of toughening in abalone shells and translation to synthetic composite materials. *Nat. Commun.* 2, 173.
- Ford, L.E., Huxley, A.F., Simmons, R.M., 1981. The relation between stiffness and filament overlap in stimulated muscle fibres. *J. Physiol.* 311, 21949.
- Fratzl, P., Weinkamer, R., 2007. Nature's hierarchical materials. *Prog. Mater. Sci.* 52, 12631334.
- Gao, H., Ji, B., Jäger, I.L., Arzt, E., Fratzl, P., 2003. Materials become insensitive to flaws at nanoscale: lessons from nature. *PNAS* 100, 5597–5600.
- Gautieri, A., Vesentini, S., Buehler, M.J., 2011. Hierarchical structure and nano-mechanics of collagen microfibrils from the atomistic scale up. *Nano Lett.* 11, 757766.
- Geoffrey, M.C., 2000. *The Cell, a Molecular Approach*. Boston University, Sunderland.
- Gibson, R.F., 2012. *Principles of Composite Materials Mechanics*. CRC Press, Taylor & Francis Group, Boca Raton.
- Gibson, L.J., Ashby, M.F., Karam, G.N., Wegst, U., Shercliff, H.R., 1995. The mechanical properties of natural materials. II. Microstructures for mechanical efficiency. *Proc. R. Soc. Lond. A* 450, 141–162.
- Giordano, S., 2003. Differential schemes for the elastic characterization of dispersions of randomly oriented ellipsoids. *Eur. J. Mech. A/Sol* 22, 885–902.
- Giordano, S., 2005. Order and disorder in heterogeneous material microstructure: electric and elastic characterisation of dispersions of pseudo-oriented spheroids. *Int. J. Eng. Sci.* 43, 1033–1058.
- Giordano, S., Colombo, L., 2007. Effects of the orientational distribution of cracks in isotropic solids. *Eng. Frac. Mech.* 74, 1983–2003.
- Giordano, S., Colombo, L., 2007. Effects of the orientational distribution of cracks in solids. *Phys. Rev. Lett.* 98, 055503.
- Golub, G.H., Van Loan, C.F., 1996. *Matrix Computations*. Johns Hopkins, Baltimore and London.
- Griffith, A.A., 1920. The phenomena of rupture and flow in solids. *Phil. Roy. Soc. Lond. A* 221, 163.
- Hamrell, B.B., Hultgren, P.B., 1992. Reduced isotonic sarcomere shortening in rabbit right ventricular pressure overload hypertrophy. *J. Mol. Cell. Cardiol.* 24, 133147.
- Hodge, A.J., Schmitt, F.O., 1960. The charge profile of the tropocollagen macromolecule and the packing arrangement in native-type collagen fibrils. *Proc. Natl. Acad. Sci.* 46, 186197.
- Holmes, D.F., Gilpin, C.J., Baldock, C., Ziese, U., Koster, A.J., Kadler, K.E., 2001. Corneal collagen fibril structure in three dimensions: structural insights into fibril assembly, mechanical properties, and tissue organization. *PNAS* 98, 7307–7312.
- Huang, X., Liu, G., Wang, X., 2012. New secrets of spider silk: exceptionally high thermal conductivity and its abnormal change under stretching. *Adv. Mater.* 24, 1482–1486.
- Hulmes, D.J.S., Wess, T.J., Prockop, D.J., Fratzl, P., 1995. Radial packing, order, and disorder in collagen fibrils. *Biophysical J.* 68, 1661–1670.
- Hutchinson, J.W., Jensen, H.M., 1990. Model of fiber debonding and pullout in brittle composites with friction. *Mech. Mater.* 9, 139–163.
- Irwin, G., 1957. Analysis of stresses and strains near the end of a crack traversing a plate. *J. Appl. Mech.* 24, 361364.
- Jackson, A., Vincent, J., Turner, R., 1988. The mechanical design of nacre. *Proc. R. Soc. Lond. B Biol. Sci.* 234, 415440.
- Jacot, J.G., Kita-Matsuo, H., Wei, K.A., Chen, H.S.V., Omens, J.H., Mercola, M., McCulloch, A.D., 2010. Analysis of Cardiac Development Cardiac myocyte force development during differentiation and maturation. *Ann. N.Y. Acad. Sci.* 0077–8923.
- Jäger, I., Fratzl, P., 2000. Mineralized collagen fibrils: a mechanical model with a staggered arrangement of mineral particles. *Biophysical J.* 79, 1737–1746.
- Ji, B., Gao, H., 2004. Mechanical properties of nanostructure of biological materials. *J. Mech. Phys. Solids* 52, 1963–1990.
- Kachanov, M., 1992. Effective elastic properties of cracked solids: critical review of some basic concepts. *Appl. Mech. Rev.* 45, 305.
- Kachanov, M., 1994. Elastic solids with many cracks and related problems. *Adv. Appl. Mech.* 30, 259.
- Kachanov, M., Sevostianov, I., 2005. On quantitative characterization of microstructures and effective properties. *Int. J. Sol. Struct.* 42, 309–336.
- Kanaun, S., Levin, V., 2008. *Static Problems. Self-consistent Methods for Composites*, 1. Springer, Dordrecht.
- Kanaun, S., Levin, V., 2008. *Wave Propagation in Heterogeneous Materials. Self-consistent Methods for Composites*, 2. Springer, Dordrecht.
- Kawai, M., Brandt, P.W., 1980. Sinusoidal analysis: a high resolution method for correlating biochemical reactions with physiological processes in activated muscles of rabbit, frog and crayfish. *J. Muscle Res Cell Motil* 1, 279303.
- Kawamura, H., Hatano, T., Kato, N., Biswas, S., Chakrabarti, B.K., 2012. Statistical physics of fracture, friction, and earthquake. *Rev. Mod. Phys.* 84, 839.
- Keten, S., Xu, Z., Ihle, B., Buehler, M.J., 2010. Nanoconfinement controls stiffness, strength and mechanical toughness of β -sheet crystals in silk. *Nat. Mater.* 9, 359–367.
- Kojima, H., Ishijima, A., Yanagida, T., 1994. Direct measurement of stiffness of single actin filaments with and without tropomyosin by in vitro nanomanipulation. *Proc. Natl. Acad. Sci. U. S. A.* 91, 12962–12966.
- Kossmann, C.E., Huxley, H.E., 1961. The contractile structure of Cardiac and skeletal muscle. *Circulation* 24, 328–335.
- Lagoudas, D.C., Hui, C.Y., Phoenix, S.L., 1989. Time evolution of overstress profiles near broken fibers in a composite with a viscoelastic matrix. *Int. J. Solids Struct.* 25, 45.
- Landis, W., Song, M., Leith, A., McEwen, L., McEwen, B., 1993. Mineral and organic matrix interaction in normally Calcifying tendon visualized in three dimensions by HighVoltage electron microscopic tomography and graphic image reconstruction. *J. Struct. Biol.* 110, 3954.
- Lei, H.F., Zhang, Z.Q., Liu, B., 2012. Effect of fiber arrangement on mechanical properties of short fiber reinforced composites. *Compos. Sci. Technol.* 72, 506–514.
- Lei, H.J., Zhang, Z.Q., Han, F., Liu, B., Zhang, Y.W., Gao, H.J., 2013. Elastic bounds of bioinspired nanocomposites. *J. Appl. Mech.* 80, 061017.
- Lin, A., Meyers, M.A., 2005. Growth and structure in abalone shell. *Mater. Sci. Eng. A* 390, 2741.
- Mahesh, S., Phoenix, S.L., 2004. Lifetime distributions for unidirectional fibrous composites under creep-rupture loading. *Int. J. Fract.* 127, 303–360.
- Manca, F., Giordano, S., Palla, P.L., Zucca, R., Cleri, F., Colombo, L., 2012. Elasticity of flexible and semiflexible polymers with extensible bonds in the Gibbs and Helmholtz ensembles. *J. Chem. Phys.* 136, 154906.
- Manca, F., Giordano, S., Palla, P.L., Cleri, F., Colombo, L., 2012. Theory and Monte Carlo simulations for the stretching of flexible and semiflexible single polymer chains under external fields. *J. Chem. Phys.* 137, 244907.
- Manca, F., Giordano, S., Palla, P.L., Cleri, F., Colombo, L., 2013. Two-state theory of single-molecule stretching experiments. *Phys. Rev. E* 87 (032705).
- Manca, F., Giordano, S., Palla, P.L., Cleri, F., 2014. Scaling shift in multicracked fiber bundles. *Phys. Rev. Lett.* 113, 255501.
- Manca, F., Giordano, S., Palla, P.L., Cleri, F., 2014. On the equivalence of thermodynamics ensembles for flexible polymer chains. *Phys. A Stat. Mech. its Appl.* 395, 154.
- Manca, F., Giordano, S., Palla, P.L., Cleri, F., 2015. Stochastic mechanical degradation of multi-cracked fiber bundles with elastic and viscous interactions. *Eur. Phys. J. E* 38, 44.
- Mason, D.D., Hui, C.Y., Phoenix, S.L., 1992. Stress profiles around a fiber break in a composite with a nonlinear, power law creeping matrix. *Int. J. Solids Struct.* 29, 2829.
- Meyers, M.A., Chen, P.-Y., Lin, A.Y.-M., Seki, Y., 2008. Biological materials: structure and mechanical properties. *Prog. Mater. Sci.* 53, 1206.
- Milton, G.W., 2002. *The Theory of Composites*. Cambridge University Press, Cambridge.
- Moore, E.H., 1920. On the reciprocal of the general algebraic matrix. *Bull. AMS* 26, 394–395.
- Nairn, J.A., 1997. On the use of shear-lag methods for analysis of stress transfer in unidirectional composites. *Mech. Mater.* 26, 63–80.
- Ni, Y., Song, Z., Jiang, H., Yu, S.-H., He, L., 2015. Optimization design of strong and tough nacreous nano-composites through tuning characteristic lengths. *J. Mech. Phys. Solids* 81, 41–57.
- Nikolov, S., Raabe, D., 2008. Hierarchical modeling of the elastic properties of bone at submicron scales: the role of extracellular mineralization. *Biophys. J.* 94, 42204232.
- Okumura, K., de Gennes, P.-G., 2001. Why is nacre strong? Elastic theory and fracture mechanics for biocomposites with stratified structures. *Eur. Phys. J. E* 4, 121–127.
- Orgel, J.P., Miller, A., Irving, T.C., Fischetti, R.F., Hammersley, A.P., Wess, T.J., 2001. The in situ supermolecular structure of type I collagen. *Structure* 9, 10611069.
- Peirce, F.T., 1926. Tensile tests for cotton yarns. "The weakest link" theorems on the strength of long and of composite specimens. *J. Text. Inst.* 17, T355–T368.
- Penel, S., Morrison, R.G., Dobson, P.D., Mortishire Smith, R.J., Doig, A.J., 2003. Length preferences and periodicity in strands. Antiparallel edge sheets are more likely to finish in non hydrogen bonded rings. *Protein Eng.* 16, 957–961.
- Penrose, R., 1955. A generalized inverse for matrices. *Proc. Camb. Philos. Soc.* 51, 406–413.

- Pontryagin, L.S., 1962. *Ordinary Differential Equations*. Addison-Wesley, New York.
- Pradhan, S., Hansen, A., Chakrabarti, B.K., 2010. Failure processes in elastic fiber bundles. *Rev. Mod. Phys.* 82, 499.
- Qu, J., Cherkaoui, M., 2006. *Fundamentals of Micromechanics of Solids*. John Wiley Sons, New Jersey.
- Ramachandran, G.N., Kartha, G., 1955. Structure of collagen. *Nature* 176, 593595.
- Satcher Jr., R.L., Forbes Jr., D., 1996. Theoretical estimates of mechanical properties of the endothelial cell Cytoskeleton. *Biophysical J.* 71, 109–118.
- Shao, Y., Zhao, H.-P., Feng, X.-Q., 2014. Optimal characteristic nanosizes of mineral bridges in mollusk nacre. *RSC Adv.* 4, 32451.
- Smith, B.L., Schaffer, T.E., Viani, M., Thompson, J.B., Frederick, N.A., Kindt, J., Belcher, A., Stucky, G.D., Morse, D.E., Hansma, P.K., 1999. Molecular mechanistic origin of the toughness of natural adhesives, fibres and composites. *Nat. Lond.* 399, 761.
- Sun, J., Bhushan, B., 2012. Hierarchical structure and mechanical properties of nacre: a review. *RSC Adv.* 2, 76177632.
- Sun, Y., Luo, Z., Fertala, A., An, K., 2002. Direct quantification of the flexibility of type I collagen monomer. *Biochem. and Biophysical Res. Commun.* 295 (2), 382–386.
- Sun, X.Y., Zhang, Z.Q., Xu, Y.J., Zhang, Y.W., 2015. An elastic model for bioinspired design of carbon nanotube bundles. *Acta Mech. Sin.* 31, 205–215.
- Tang, H., Barthelat, F., Espinosa, H., 2007. An elasto-viscoplastic interface model for investigating the constitutive behavior of nacre. *J. Mech. Phys. Solids* 55, 14101438.
- Tedesco, F.S., Dellavalle, A., Diaz-Manera, J., Messina, G., Cossu, G., 2010. Repairing skeletal muscle: regenerative potential of skeletal muscle stem cells. *J. Clin. Investigation* 120, 11–19.
- Thomas, J.B., Richard, L.L., 2001. Sarcomere length operating range of vertebrate muscles during movement. *J. Exp. Biol.* 204, 15291536.
- Torquato, S., 2002. *Random Heterogeneous Materials*. Springer-Verlag, New York.
- Van Beek, J.D., Hess, S., Vollrath, F., Meier, B.H., 2002. The molecular structure of spider dragline silk: folding and orientation of the protein backbone. *PNAS* 99 (16), 10266–10271.
- Van Loan, C.F., 1978. Computing integrals involving the matrix exponential. *IEEE Transaction Automatic Control* AC-23, 395.
- Wada, H., Tanaka, Y., 2011. Mechanics and size-dependent elasticity of composite networks. *Erratum, 2011 Europhys. Lett.* 95, 29901.
- Walpole, L.J., 1981. Elastic behavior of composite materials: theoretical foundations. *Adv. Appl. Mech.* 11, 169242.
- Wei, X., Naraghi, M., Espinosa, H.D., 2012. Optimal length scales emerging from shear load transfer in natural materials: application to carbon-based nanocomposite design. *ACS-Nano* 6, 2333–2344.
- Weijts, W.A., van der Wielen, A., Drent, T.K., 1983. The relationship between sarcomere length and activation pattern in the rabbit masseter muscle. *Arch. Oral Biol.* 28, 307315.
- Yang, L., Van Der Werf, K.O., Fiti, C.F.C., Bennink, M.L., Dijkstra, P.J., Feijen, J., 2008. Mechanical properties of native and cross-linked type I collagen fibrils. *Biophys. J.* 94, 22042211.
- Yao, H., Dao, M., Carnelli, D., Tai, K., Ortiz, C., 2011. Size-dependent heterogeneity benefits the mechanical performance of bone. *J. Mech. Phys. Solids* 59, 64–74.
- Zhang, Z.Q., Liu, B., Huang, Y., Hwang, K.C., Gao, H.J., 2010. Mechanical properties of unidirectional nanocomposites with non-uniformly or randomly staggered platelet distribution. *J. Mech. Phys. Solids* 58, 1646–1660.
- Zhang, Z.Q., Liu, B., Zhang, Y.W., Hwang, K.C., Gao, H.J., 2014. Ultra-strong collagen-mimic carbon nanotube bundles. *Carbon* 77, 1040–1053.